Thermal fluid modelling of a titanium fluted tube condenser

MM Jordaan

orcid.org/ 0000-0002-0024-2814

Dissertation accepted in fulfilment of the requirements for the degree *Master of Engineering in Mechanical Engineering* at the North West University

Supervisor: Mr CP Kloppers

Co-supervisor: Prof M van Eldik

Graduation: June 2021

Student number: 24907928

ACKNOWLEDGEMENTS

Throughout the writing of this dissertation I have received numerous support and assistance and I am thankful for everyone who contributed in some sort.

Firstly, I would like to thank my two study leaders for their mentorship and support.
Secondly, I would like to thank Christiaan de Wet from Aerotherm, for his assistance an mentorship in simulation solving, his knowledge in CFD made this dissertation possible.
Thank you for my parents who always motivated me to reach my goals and to my Heavenly Father who has blessed me with the ability to complete this dissertation.
Lastly to my fiancé Thehann van Niekerk, who helped me keep on track with my dissertation throughout Covid-19 lockdown and keeping me sane throughout the process.

ABSTRACT

Heat exchangers form a vital component in numerous energy conversion processes, ranging over multiple industries; such as mining, food, automotive and aerospace. With the continuous population growth and a drive towards more efficient energy consumption, there exists a persistent need to improve heat exchangers. Over the past decade research focused on improving the internal convective heat transfer of tubes by means of spiral flutes or grooves. Fluted tubes gained popularity in the industry as the spiral flutes increase the heat transfer by disrupting the boundary layer at the tube surface. Spiral fluted condensers are used in water heating heat pumps which are widely applied in the industry to reduce the overall electricity consumption of a facility.

Due to a fluted tube's complex geometry and manufacturing challenges, additive manufacturing may be a solution for improving on conventional methods. This study investigates the effect of altering the flute pitch and flute depth on the thermal performance of a titanium helically coiled fluted tube heat exchanger, focusing on the internal fluid.

In attaining the latter, computational fluid dynamic software STAR-CCM+ is utilised to simulate the enhancements of the heat exchanger. For the mesh selection, a grid verification index is performed, and the physics model utilises the K-Epsilon approach with segregated flow.

Sixteen different configurations were modelled where each comprise a different depth and pitch combination. The flute pitch and depth vary from 9mm to 12mm, and 4.59mm to 7.17mm respectively.

The results indicate, that with an increase in flute depth, the thermal performance and the pressure drop both increases. Increasing the flute pitch, results in a decrease in pressure drop and thermal performance. It is concluded that flute depth and pitch have a significant effect on the thermal performance of the internal fluid. The enhancement comprising a flute depth and pitch of 7.17mm and 9mm respectively resulted in the highest Nusselt number.

Finally, the effect of altering from pure titanium to Titanium-6 Aluminium-4 Vanadium additively manufactured material was investigated and compared against the enhancement with the highest thermal performance. This led to a decrease in 8.97% in Nusselt number when compared to pure titanium.

Key words: Fluted tube, Helically coiled fluted tube, heat exchangers, enhancements, computational fluid dynamics, simulation, turbulent flow

TABLE OF CONTENTS

LIST OF TABLES

LIST OF FIGURES

ACRONYMS

Helically Coiled Fluted tube heat exchanger	HCFT-HX
Additive Manufacturing	AM
Computational Fluid Dynamic	CFD
Titanium-6-Aluminium-4-Vanadium	Ti64
three-dimensional	3D
Standard Tessellation Language file format	.STL
Powder Based Fusion	PBF
Directed Energy Deposition	DED
Selective Laser Melting/Sintering	SLM/SLS
Laser Cutting	LC
Electron Beam Melting	EBM
Laser Engineered Net Shaping	LENS
Direct Metal Deposition	DMD
Electron Beam Free Form Fabrication	EBFFF
Computer Tomography	CT
Computer Aided Design	CAD
Baseline Traditionally manufacture	BTM
Baseline AM	BAM
Enhanced Traditionally manufactured	ETM
Enhanced AM	EAM

control volume	CV
Reynold-Average Navier-Stokes	RANS
Engineering Equation Solver	EES
finite element	FE
finite volume	FV
Grid Verification Index	GVI

CHAPTER 1: INTRODUCTION

This chapter provides a brief background in what a titanium fluted condenser is and the importance of creating a thermal fluid simulation of the device.

1.1 Background

Heat exchangers form a vital component in numerous energy conversion processes, ranging over multiple industries; such as mining, food, automotive and aerospace. With the continuous population growth and a drive towards more efficient energy consumption, there exists a persistent need to improve heat exchangers [1], [2]. Presently, a significant amount of research has been conducted in identifying alternative methods that may increase heat exchanger efficiency. Over the past decade research focused on improving the internal convective heat transfer of tubes by means of spiral flutes or grooves.

Fluted tubes have gained a higher interest from industry, owing to the spiral flutes' ability to increase heat transfer by disrupting the boundary layer at the tube surface [3]. This augmentation is more commonly used in tube-in-tube condensers (also known as helically coiled fluted tube heat exchangers) that are found in heat pump systems as illustrated in Figure 1-1 below [4]. Heat pump systems are widely used for commercial and industrial applications to reduce the total electricity consumption of a facility [4]. The condenser forms a critical component of the vapour compression cycle, and thus the overall efficiency of the system is dependent on the effectiveness thereof [5].

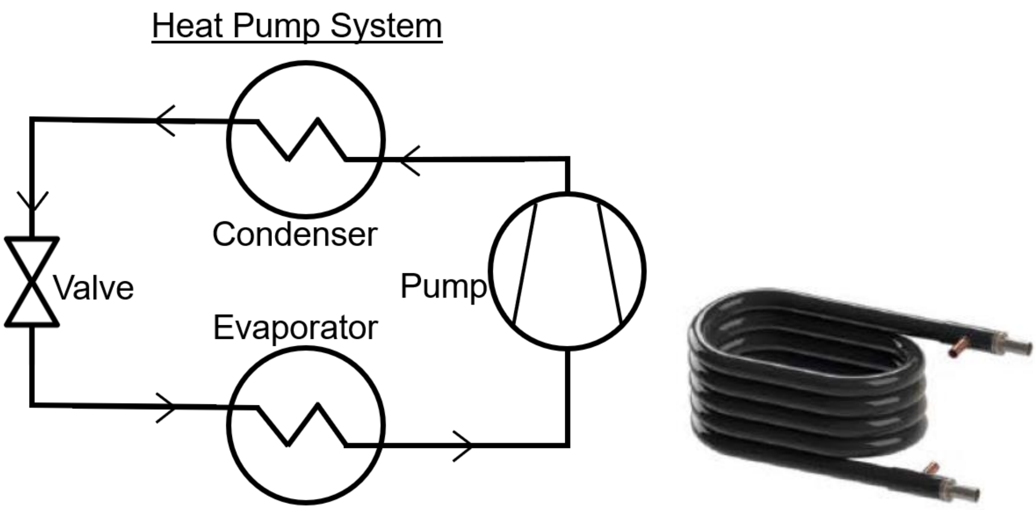

Figure 1-1: Illustration of water heating heat pump (left) and a helically coiled fluted tube heat exchanger with 4.5 coil revolutions(right)

Literature on the enhancements of a Helically Coiled Fluted tube heat exchanger (HCFT-HX) is limited when compared to straight fluted tubes. Enhancing the thermal performance of a fluted tube consists of altering any one of the following parameters;

- Flute pitch (the amount of revolutions the cross-sectional geometry makes per meter).
- Flute depth as illustrated in Figure 1-2.
- Number of starts as illustrated in Figure 1-2.

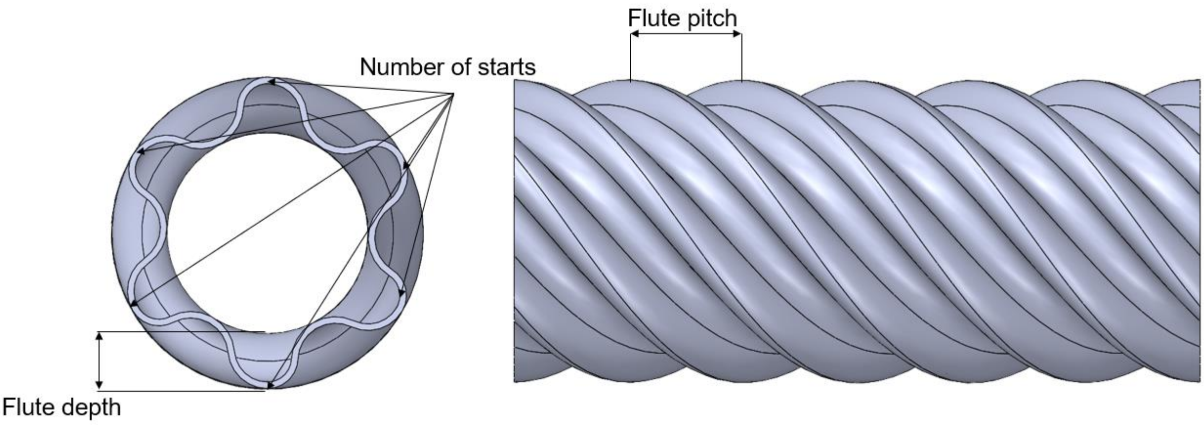

Figure 1-2: Fluted tube illustration of its parameters

Owing to the complex manufacturing of a HCFT-HX, manufacturing any alterations/enhancements on the parameters (flute dept and flute pitch) through traditional methods are lost. Figure 1-3 presents a traditionally manufactured copper HCFT-HX's cross-section, identifying the inconsistent flute depth in the curvature of the helical coil pack. Additional manufacturing complications arise when the internal tube is manufactured with titanium to better suit the use of process water, since it is resistant to fouling and has high corrosion fatigue [6]. Titanium alloys are recognised for its lightweight, hardness and corrosion resistance, however, using titanium alloys to manufacture complex geometry through traditional technologies are exceedingly challenging [7].

Inconsistency of cross-section in curvature of pipe.

Figure 1-3: Cross-section of a copper HCFT-HX manufactured using traditional technology.

A possible solution to manufacture improvements on heat exchangers with complex geometry, is to opt for alternative manufacturing techniques. As a response, the study argues that Additive Manufacturing (AM) may be employed to address the manufacturing of complex geometry. The potential advantage of AM over traditional techniques is the ability to manufacture heat exchangers as a single component [8]. Together with the advantage of eliminating assembly, parameter accuracies may be efficiently controlled throughout the entire device [8]. Currently, limited literature is available on the thermal performance of a titanium HCFT-HX and how the parameters (as illustrated in Figure 1-4) affect the convective heat transfer of the internal fluid.

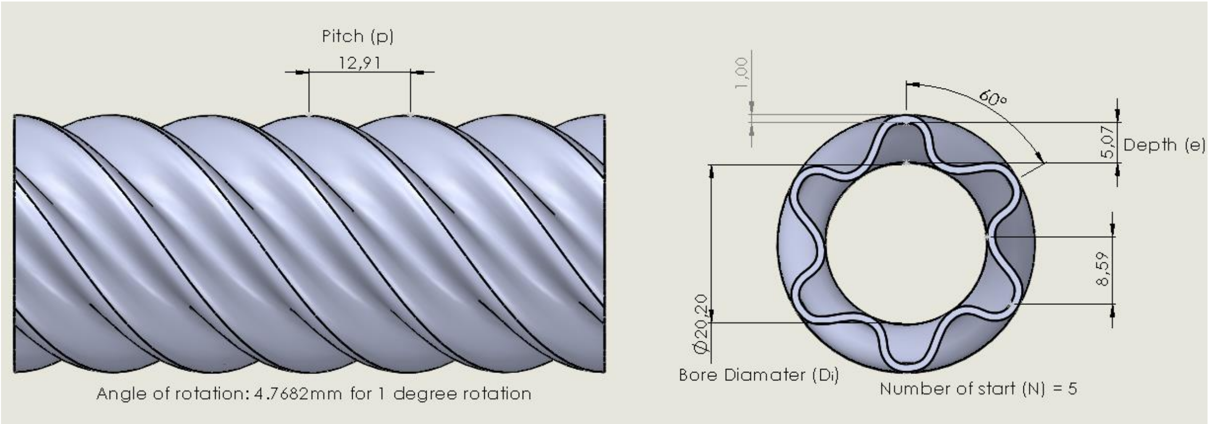

Figure 1-4: Six-start spirally fluted tube and its parameters namely flute pitch, number of starts, flute depth, length, bore diameter and envelope diameter [own creation].

1.2 Problem statement

Industry is continuously striving for more efficient heat exchangers. With the titanium HCFT-HX being an innovative solution, increasing its performance by using AM will be beneficial to multiple industries. Current research on the effect of heat transfer by varying the fluted geometry is limited, and more specifically understanding the fluid particle flow as it moves through the complex area.

1.3 Purpose of the study

The purpose of this study is to determine the effect of flute depth and pitch on the inner fluid's thermal performance of a HCFT-HX. This will be accomplished by simulating the enhanced heat exchanger in Computational Fluid Dynamic (CFD). Furthermore, the study will evaluate whether manufacturing the HCFT-HX with Titanium-6-Aluminium-4-Vanadium (Ti64) through AM may improve the heat exchanger's thermal performance.

1.4 Aim and objectives

In exploring the latter, a thermal-fluid model has to be constructed of the HCFT-HX in order to simulate the enhancements accordingly. To develop the thermal fluid model of the HCFT-HX, the following objectives have been formulated:

- Investigate literature with regards to the effect that the flute depth and pitch have on the thermal performance of the fluted tube.
- Develop a CFD model to accurately predict the thermal performance of the inner fluid in a HCFT-HX.
- Validate the simulated HCFT-HX with data obtained from an experimental study.
- Conclude whether the manufacturing of the enhancements through AM and utilising Ti64, may be beneficial.

1.5 Limitations of the study

- Computational power and time; to simulate of the HCFT-HX as a complete component is computationally expensive and tedious due to the large size of the heat exchanger. The alternative is to simulate a single revolution of the heat exchanger.
- Printing capabilities; AM technology in South Africa is still in the beginning phase. As a result, the HCFT-HX will not be manufactured, only simulations will be conducted.

CHAPTER 2: LITERATURE REVIEW

This chapter comprises an overview of fluted tube heat exchangers and additive manufacturing in addition to an in-depth review of recent, relevant research in the field of focus.

2.1 Fluted tube heat exchanger

Research on enhanced surfaces and its effects on the thermodynamic performance of heat exchangers date back to the 1950's [9]. Currently, it is an area of interest as can be seen by the published research over the past decade. One such surface enhancement is the fluted tube, also known as a spirally corrugated tube or coaxial coil. In this section a detailed literature review is conducted to evaluate relevant research on fluted or spirally corrugated tubes.

2.1.1 Introduction

During 1954, Gregorig proposed that surface tension should be utilised to enhance laminar film condensation, and is currently known as the Gregorig effect [9], [10]. The research indicates that helical grooves, on a vertical surface, induce surface tension and enhance condensation by 2 to 8 times when compared to smooth surfaces [11]. Since the discovery of the Gregorig effect, research in utilising flutes in various heat exchangers have gained popularity, owing to its ability to generate secondary flow via radial velocities and mixing of the flow layer. An existing heat exchanger that readily employs flute is the tube-in-tube heat exchanger that comprises a fluted internal tube [12]. This type of heat exchanger became commonly known as a fluted tube heat exchanger, also known as a coaxial coil or spirally corrugated heat exchanger. Fluted tubes are generally coiled into a pack, minimising the amount of space the heat exchanger occupies, while enhancing thermal performance. This thermal enhancement is a result of gravitational force that induces secondary flow in the internal fluid. Consequently, secondary flow encourages high turbulence that enhances the heat transfer. Ensuing Figure 2–1 illustrates secondary flow in a circular pipe [13].

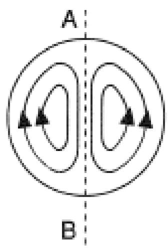

Figure 2-1: Illustration of secondary flow in a circular pipe.

2.1.2 Influence of fluted tube geometry on heat transfer and pressure drop.

As stated in Chapter 1, the main characteristics of a fluted tube are the flute pitch p, flute depth e, the bore diameter D_i, number of starts N, and the angle of rotation θ . The characteristics are illustrated in Figure 2-2 below.

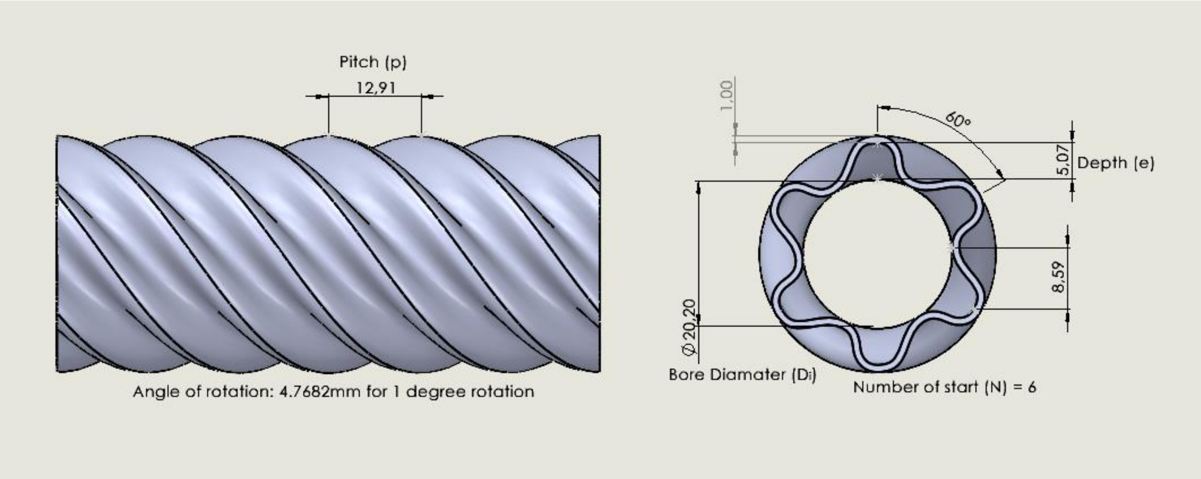

Figure 2-2: Parameters of a fluted tube [own creation]

In recent years, fluted tubes are investigated due to its combined merits of extended surfaces, turbulators and roughness [14]. Nazir *et al*. [15] investigate the effect flute profile has on heat transfer enhancements focusing on the laminar flow region (Reynolds numbers ranging from 100-1300). Their study comprises a horizontally orientated straight fluted tubes, the three geometrical profiles that the study compared against a smooth tube are classified as circular, waved and curved flute profiles as illustrated in Figure 2-3 below.

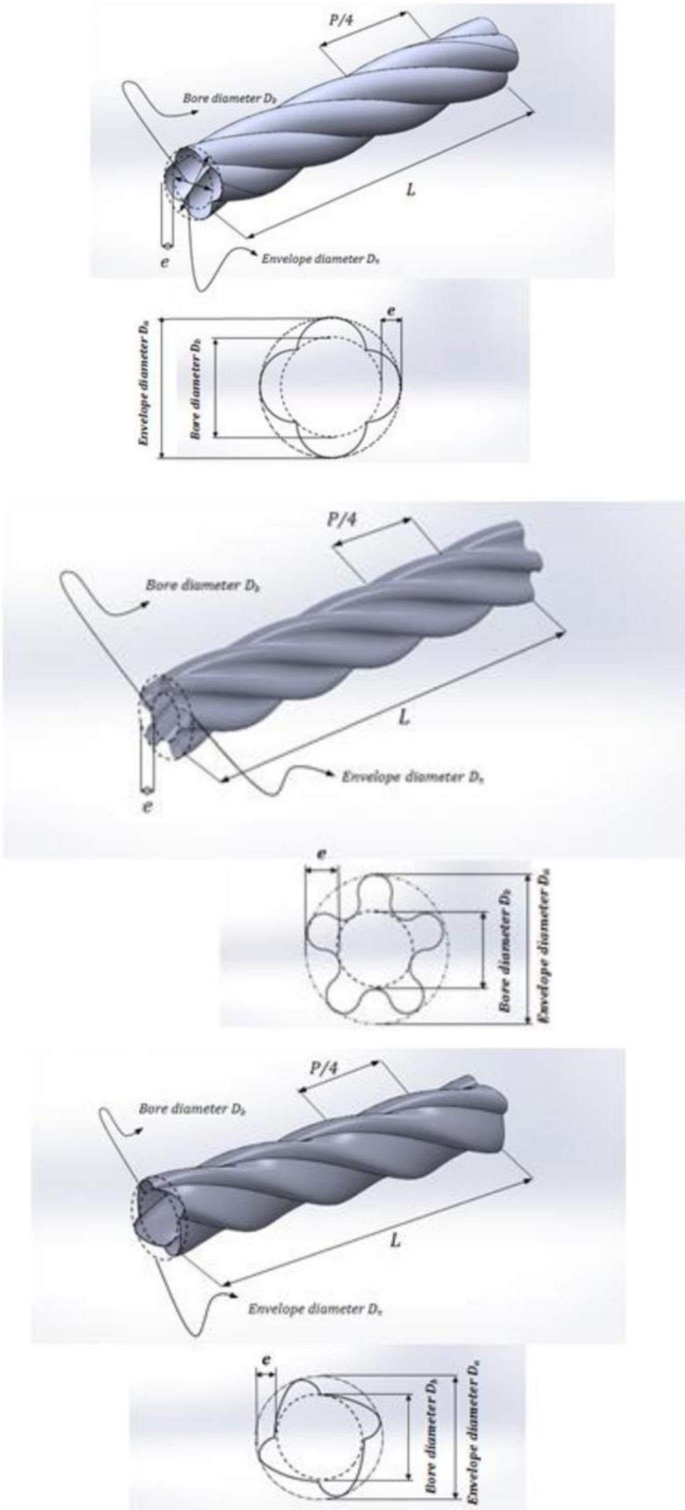

Figure 2-3: Flute profile as depicted in Nazir et al.'s work [15]**.**

The study implements identical characteristic parameters, namely; flute depth over diameter and pitch over diameter in all three geometries to ensure consistency. The study utilises CFD and simulated the tubes with a heat flux on the outer wall and an internal flow configuration.

The assessment criteria are based on the comparison between the Nusselt number of the different tubes. Interestingly, no significant increase in heat transfer is found at the lower end of Reynolds numbers in any of the fluted profiles. However, at the upper regions of the study's Reynolds numbers, it is identified that the curved flute geometry has the best performance, considering that it offers smooth successive corrugation for the flow with the continuous contact of fluid layers to the tube wall.

The heat transfer results of the three profiles, when compared to a smooth tube, are as follows: circular flute has a 13.8% to 22.17% increase, waved flute has a 15.7% to 30.5% increase and the curved flute has a 18.4% to 36.3% increase for Reynolds numbers between 100 and 1000 [15]. From this study, it may be concluded that higher Reynolds numbers provide an increase in heat transfer when compared to low Reynolds numbers. In conclusion, an estimation can be drawn on how the geometrical profile may be adjusted to enhance the heat transfer [15].

As mentioned, the research of Nazir *et al*. [15] conducted tests in the lower Reynolds number region (100<Re<1300), however, practical applications of heat exchangers mostly operate at high Reynolds numbers (2300<Re). Kongkaitpaiboon *et al*. [16] investigate the effect that the number of flute starts have on the performance of a heat exchanger in turbulent flow conditions [16]. The study explores a similar profile than the circular spiral flute profile in Nazir *et al*. [15] study as illustrated in Figure 2-4.

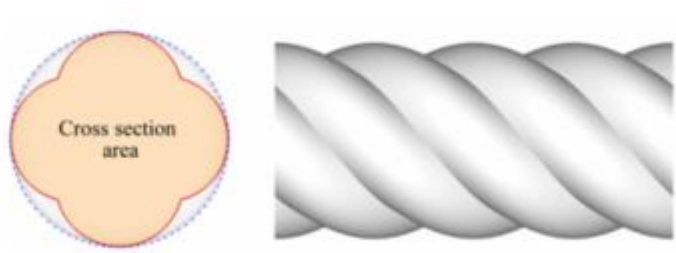

Figure 2-4: Four start spirally corrugated tube investigated in Kongkaitpaiboon et al.'s work [15].

Kongkaitpaiboon *et al*. [16] examine the effect that the number of flute starts and flute depth ratio (flute depth over hydraulic diameter) have on the heat transfer rate, flow structure and flow friction. The study is conducted in the turbulent region of flow with Reynolds numbers consisting of 5000, 8000, 14000 and 20000 [16].

The study determines that with an increase of the amount of spiral starts, the Nusselt number increases. The scholars identify that this increase may be attributed to the strong swirl flow. It is stated that the relation between the Nusselt number for tubes consisting of 4 and 5 flute starts, is depended on the depth ratio, given that heat transfer depends on the interaction between two effects, namely; the positive effect and the negative effect.

The positive effect is the strong swirl flow, associated with the increase in depth ratio and the number of starts that consequently increases turbulence. The negative effect is the difficulty for the fluid to transfer into the grooves due to the increase in depth ratio and complex geometry, resulting in the increase in pressure drop over the pipes. The study uses a thermal evaluation performance (TEF) factor to compare the performance of the different cases. The equation to determine the TEF of an experimental test is illustrated in equation 2-1. With Nu, Nu_o and f, f_o being the Nusselt number and friction factor for the enhanced tube and a straight tube respectively.

$$\boldsymbol{TEF} = \frac{\frac{Nu}{Nu_o}}{\left(\frac{f}{f_o}\right)^{\frac{1}{3}}} \quad \textbf{[2-1]}$$

The TEF of the study ranges from 0.66 to 1.2 when compared to straight tubes, considering that a straight tube is the base line for TEF. The highest TEF (1.2) is obtained by the tube comprising four flute starts with a depth ratio of 0.08 and a Reynolds number of 5000 [16]. Addiotinally, the increase in Nusselt numbers and friction factors, when corrugated tubes are compared to smooth tubes, ranged from 0.82 to 2.16 and 1 to 8.26, respectively. In considering this study, it is important to conclude that the depth ratio, coupled with the number of starts play a pivotal role in the thermal enhancement and the pressure drop [16].

In the contributing article to Nazir *et al*. [15], Lazim *et al*. [14] conduct a CFD thermal fluid modelling study of a horizontal circular flute tube to investigate the heat transfer capabilities. The four start spirally fluted tube is investigated, indicating that the pitch to diameter and the flute depth to diameter have the greatest effect on the heat transfer enhancement as they act as smooth repeated disturbances for the fluid layers that produce swirl.

Ya-xia *et al*. [17] examine the heat transfer and fluid flow characteristics of a spirally corrugated helical tube. When compared to the above-mentioned studies, this study incorporates the helical characteristic of the heat exchanger, whereas the previous studies focus on straight sections of spirally corrugated tubes. As previously stated, the benefit that helical tubes possess over straight tubes is secondary flow generation in the internal fluid that are caused by centrifugal forces. This provides effective mixing of the fluid, while enhancing the heat transfer performance of the device [17]. Helical coils have a significant space saving benefit in addition to material savings when compared with straight tubes [18], [17]. In the study of

Ya-xia *et al*. [17], a single start spirally corrugated helical tube is investigated that is illustrated in Figure 2-5 below.

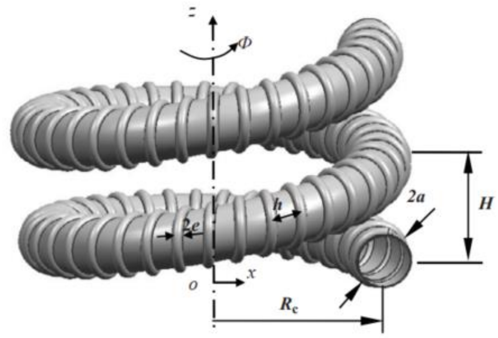

Figure 2-5: 3D model of Ya-xia *et al*.'s study [17]**.**

The study concludes that the heat transfer may be enhanced by between 50% to 80% when compared to smooth helical tubes, however, an increase in friction factor of between 50% and 300% is observed. This indicates that research is required to determine whether the parameters may be manipulated in a manner that limits the friction factor increase, while still achieving the improved heat transfer.

The study of Zhi-jiang *et al.* [19] investigates the effect that the pitch and depth of the flutes have on the heat transfer characteristics of a six-start spirally fluted tube. The study determines that the reduction of the pitch is conducive to an increase in heat transfer performance. Calculations on how the flow resistance and heat transfer compares with a smooth tube identify that the fluted tube has an increase in heat transfer performance of 1.05 to 1.33 times when compared to a smooth tube. Similarly, the friction factor/resistance coefficient of the fluted tube is between 1.5 and 2.41 times higher than the smooth tube [19]. For an increased understanding of how the pitch affects the flow field, the study maintains the cross-sectional area constant and altered the pitches, subsequently evaluating velocity field. The study indicates that an increase in pitch decreases the vorticity of the longitudinal vortex, implying that a smaller pitch has a greater heat transfer enhancement performance [19].

Furthermore, the study investigates the flute depth on the heat transfer performance. It is determined that an increase in the flute depth increases the heat transfer enhancement performance of the six-start spirally corrugated tube. Moreover, the enhancement of the heat transfer performance for all the tubes with different flute depths increases with an Reynolds number from 10 000 < Re < 60 000 [19]. The six-start spirally corrugated tube obtains a heat transfer enhancement of 1.004-1.363 times more than a smooth tube.

The study conducted by Balla *et al*. [20] investigates that heat transfer enhancement of a six started spirally corrugated tube in the laminar flow region. The scholars explore the effect that flute depth and pitch have on the heat transfer. Also, the study focusses on the severity index φ of the tubes that is described in equation [2-2] below, with flute depth e, flute pitch p and D_n the envelope diameter:

$$\boldsymbol{\varphi = \frac{e^2}{pD_n}} \qquad \textbf{[2-2]}$$

Five tubes with different flute pitch and depth are studied and compared to a smooth tube. The greatest thermal performance in the range of 1.8–3.4 is found to belong to the tubes with φ values of 0.2769 at Re=100–700, and η=2.6–3.4 for Re=700–1300.

Following the literature review, it is evident that the majority open literature is conducted on the viability of straight fluted tubes and in low Reynolds numbers (laminar flow) as illustrated in Table 2-1 below. However, growing research is available regarding the enhancement of straight fluted tubes, since it is considered as a more effective method to induce swirl flow than other extended surfaces [3]. The research signifies that flute depth and pitch play a significant part in the heat transfer enhancement of a fluted tube. As previously stated, the parameter enhancements are lost in the curves of a HCFT-HX as a result of the complex procedure to obtain the fluted tube cross-sectional geometry. Jin *et al*. [19] concur, stating that in order to obtain the geometry of a six start fluted tube, a tube has to undergo six processing mechanisms. This causes the price of a fluted tube to be expensive , limiting the use thereof by industries [12], [21], [22]. Therefore, the ensuing section investigates the potential of AM as an alternative approach to manufacturing heat exchangers with complex geometries.

Table 2-1: Literature review of fluted tube

Author	Inputs	Illustration	Outcomes
Dong *et al*. [23]	Compared, spirally fluted tube with smooth tubes. Fluid: Water and oil in the turbulent flow region. $e = 0.39 - 0.8mm;\ p = 10 - 12mm$	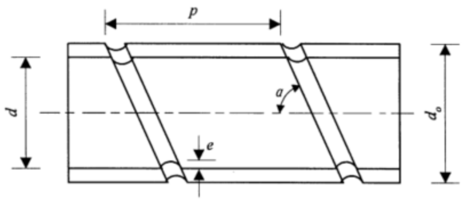	Friction factor: 60-160% increase Heat transfer: 30-120% increase
Barba *et al*. [24]	Compared, spirally fluted tube with smooth tubes. Fluid: Water in laminar region	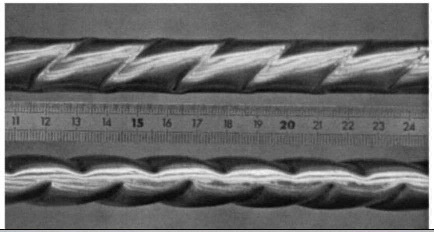	Friction factor: 1.83-2.45 increase Heat transfer: One order magnitude increase
Pethkool *et al*. [25]	Compared, corrugated tube with smooth tube. Fluid: Water in the turbulent region. $e = 0.5 - 1.5mm, p = 4.5 - 6.5mm$	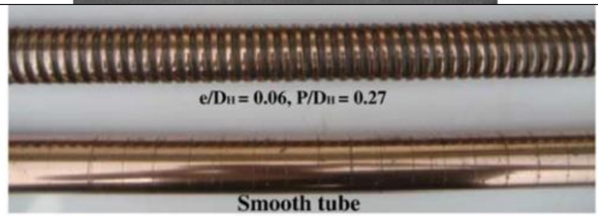	Friction factor: Increase with an increase in p/D and e/D Heat transfer: Increase with increase in p/D and e/D

Kareem *et al*. [26]	Compared, three start fluted tube to smooth tubes. Fluid: Water in laminar region. $e = 2mm, p = 10 - 50mm$	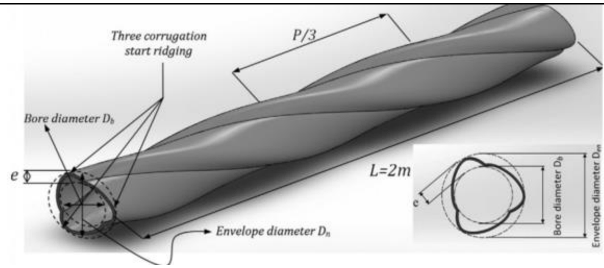	Friction Factor: 1,7-2,4 Increase Heat transfer: 2,4-3,7 Increase Pitch = 10mm has best thermal performance of 3.4 at 100<Re<1300
Kareem *et al*. [27]	Compared, three start fluted tube to smooth tubes. Fluid: Water in laminar region. $e = 1 - 3mm, p = 9 - 25mm, d_i = 19 - 22mm$	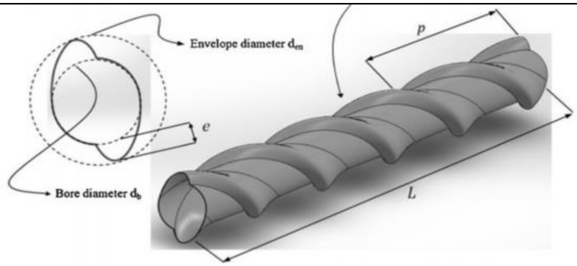	Tube with p = 9mm, e = 3mm and d_n = 22mm had best thermal performance of 1.8-2.3 .
Jin *et al.* [19]	Compares a six-start fluted tube to smooth tube. Fluid: Water in the turbulent region. $\frac{p}{d_i} = 4.07 - 5.52, \quad \frac{e}{d_i} = 0.09 - 0.28$	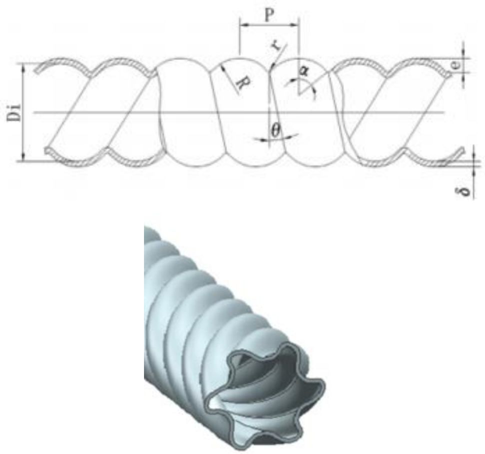	Increasing of pitch decreases the heat transfer coefficient, also the heat transfer performance of 1.05-1.33 times a smooth tube Increasing the depth increases the heat transfer coefficient, a heat transfer performance of 1.004-1.363 times a smooth tube.

Zimparov *et al.* [28]	Compared, Spirally fluted tube with smooth tubes. Fluid: Water in turbulent region $\frac{e}{d_i} = 0.44 - 1.18, \frac{p}{d_i} = 6.5 - 16.9$		Friction factor: 100-400% increase Heat transfer: 177-273% increase
Lee *et al.* [29]	Compared, Spirally fluted tube with smooth tubes. Fluid: Ethylene-glycol Water solution in Turbulent region $e = 1.6mm, p = 13mm$		Heat transfer enhancement is greater than friction factor increase. Heat transfer coefficient is 8 times higher than in smooth tubes.
Wang *et al*. [30]	Compared, Spirally fluted tube with smooth tubes. Fluid: Water in Turbulent region $e = 0.25mm, p = 15.6mm$	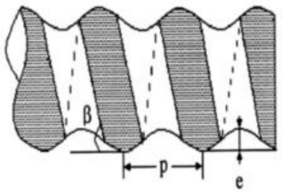	Heat transfer coefficient increased 10-17%.

2.2 Additive manufacturing and its application in thermal fluid cases.

Dilberoglu *et al*. [31] are of opinion that the current industrial revolution encourages the use and implementation of more intelligent systems for manufacturing, by considering AM as imperative component in the future of manufacturing. AM is considered as any manufacturing process that builds a three-dimensional (3D) object by adding material layer-by-layer. The manufacturing process utilises a computer and 3D modelling software to model the desired object [32]. The model is subsequently converted into a Standard Tessellation Language file format (.STL) that is fed to the printer and constructed by building each cross-sectional layer on top of each other.

In 1984, Chuck discovered the first AM technology; specifically Stereolithography, where polymer geometries are fabricated by curing a photosensitive polymer liquid with Ultra Violet (UV) laser [33]. With recent progress in computation power and material-and-modelling sciences, AM has transformed from being used exclusively for prototyping to direct part production of metallic components [34]. Metal AM is generally classified in two main groups, namely; Powder Based Fusion (PBF) based technologies and Directed Energy Deposition (DED) based technologies [35]. These two technologies can be further characterised by the type of energy source used. PBF based technologies utilise thermal energy to selectively fuse regions together on a powdered bed [35]. The main subcategories of PBF are Selective Laser Melting/Sintering (SLM/SLS), Laser Cusing (LC) and Electron Beam Melting (EBM). The DED based technologies use a Laser Engineered Net Shaping (LENS), Direct Metal Deposition (DMD), Electron Beam Free Form Fabrication (EBFFF) and arc-based AM. For the purpose of this study PBF will be further discussed; specifically, SLM, as it is currently considered as the most evolved and cost-effective AM technology[36]. Figure 2-6 provides an illustration of PBF.

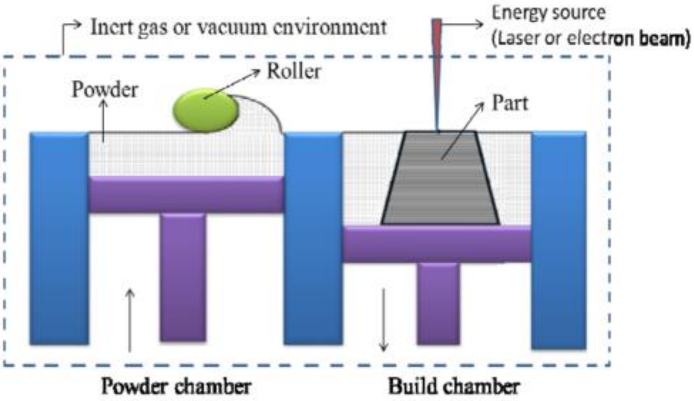

Figure 2-6: PBF process illustration [35]**.**

With regard to heat exchangers, AM is gaining popularity above traditional machining techniques due to the complex geometry it is able to manufacture [32]. In view of the latter, new heat transfer enhancement geometries are extensively investigated as it may offer unique methods that allow for integration and simplification of components, reduced manufacturing time and extend the creative design space which engineers rely on for ingenuity [22]. Supporting the aforesaid, Scheithauer *et al*. [8] list the advantages of manufacturing a heat exchanger with AM, for instance;

- Complex geometry; particularly the fluted tube, could be manufactured in a single step, since traditional manufacturing requires six successive processing mechanisms to attain a similar geometry [19].
- When a fairly complex heat exchanger is manufactured with traditional manufacturing, multiple parts is required for production and assembling. With AM highly complex heat exchangers could be manufactured in one step.
- With multiple parts, the assemble of the device could provide faults to enter the manufacturing process, while AM eliminates this limitation as it manufactures components as a whole.

In the subsequent section, numerous studies are reviewed that explored the manufacturing of heat exchangers through AM.

2.2.1 Additive Manufacturing and heat exchangers

As previously stated, AM has the potential to augment the manufacturing process of heat exchangers. In a study conducted by Seiya *et al.* [37], the feasibility of manufacturing a micro-gas heat exchanger is investigated. To determine this, the problem was sub-characterised in two smaller sections, namely; material and AM manufacturing technique. Selecting the correct material; a criteria is constructed where the maximum service temperature, density, yield strength at $600℃$, thermal conductivity at $1000℃$ and price per weight are used to analyse the materials [37]. The scholars assign the maximum service temperature and yield strength to the highest priority in material characteristics. The material selected from the wide range of available AM materials is Inconel 718, since it is considered as the optimal material to manufacture a micro gas turbine according to the study's criteria. The study concludes that AM was at that time not economically feasible, however, with technology growing at a rapid rate, AM may be economically feasible in the near future. Even though AM technology is not currently considered as the most economical viable manufacturing choice, continuous research is necessitated in to discover alternative techniques that may well enhance the feasibility to employed AM in industries.

The study conducted by Saltzman *et al*. [38] examine the effect of manufacturing a commercially available heat exchanger with AM. The study selects SLM as the manufacturing method and ALSi10Mg as the material to fabricate the heat exchanger, since it has excellent thermal conduction [39]. The study compares Airflow System Inc.'s air cooler, comprising a tube-fin geometry, with an AM replicated version. A Computer Tomography (CT) scan is done on the heat exchanger to replicate the device using AM. The heat exchanger with its Computer Aided Design (CAD) model is illustrated in Figure 2-7 below. The study notes that the layer fabrication of AM creates a "*staircase effect*" that increases the surface roughness of the walls. Owing to AM's fabrication limitation, the device may not be identically replicated, considering that the overhangs produce an inaccurate version of the air cooler. Consequently, the AM version is slightly altered as illustrated in ensuing Figure 2-7.

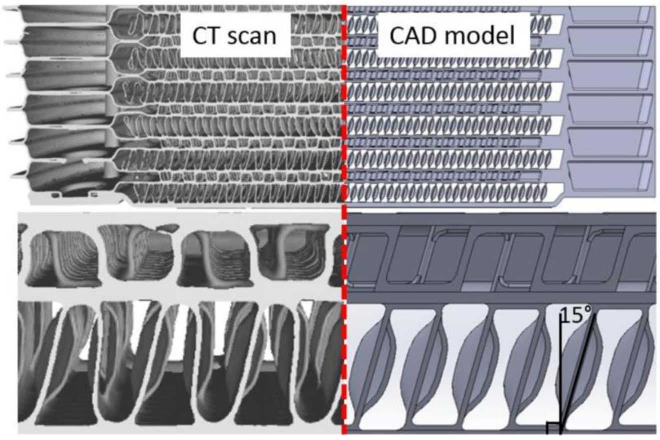

Figure 2-7: CT scan (Left) and CAD model(Right) of the device according to [24].

The study enhances the heat exchangers and therefore comprises four oil coolers namely; Baseline Traditionally manufacture (BTM), Baseline AM (BAM, Enhanced Traditionally manufactured (ETM) and Enhanced AM (EAM) and are illustrated in Figure 2-8 below.

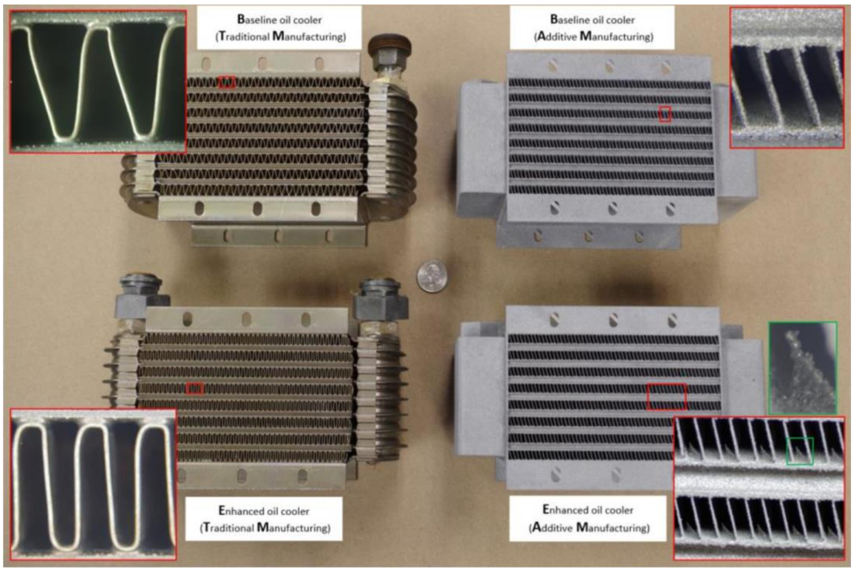

Figure 2-8: Four devices used in the study of [24].

The scholars compare the heat transfer on the liquid-side as well as the pressure drop on the air-side of these four devices under identical working condition. The BTM and ETM's pressure drop on the air side are compared to data of a manufacturing company that made it publicly available. It identifies that the pressure drop of the AM devices is significantly larger as a result of the surface roughness increase of AM. On the heat transfer on the liquid side, the BAM and EAM outperformed the BTM by over 10%. The study concludes that the AM devices outperformed the traditionally manufactured devices, yet the study recommends that "*Further* *work needs to investigate and quantify how the surface roughness affects the performance of heat transfer and pressure drop on the AM heat exchangers*." [38].

A similar study to that of Saltzman *et al*. [38] is the thesis of Garde [40] where a Case New Holland model CX55B's aluminium oil cooler is replaced with a AM replica. The study had to design, fabricate and test the oil cooler against specific conditions, for instance; a heat duty of 15kW and a pressure drop of less than 343Pa and 170kPa on the air and oil sides, respectively. In producing a design to meet the above-mentioned specifications, a lenticular tube bank with offset strip fins is selected as illustrated in Figure 2-9 below.

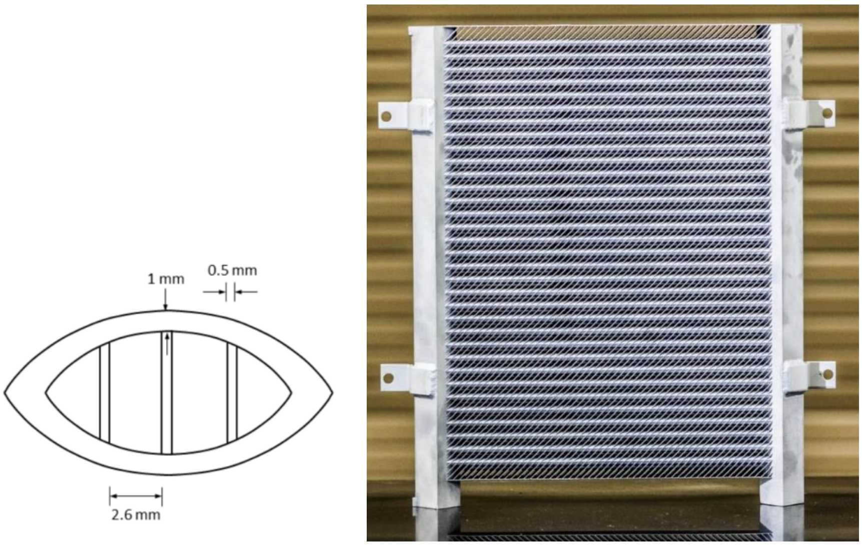

Figure 2-9: AM oil cooler with lenticular tube shapes and offset strip fins

The study states that the lenticular shape of the tubes would not have been able to be manufactured by traditional manufacturing. In validating the design, a Finite Element Analysis (FEA) is conducted. The analysis predicts that the AM oil cooler's design have an increase of 12.6667% with regard to the specified heat duty (15kW) and a pressure drop of 92Pa and 26.6kPa on the air and oil side, respectively. This study illustrates the advantages that AM may well provide heat exchangers in the future as there are currently considerable limitations in AM that outweigh their advantages.

Another advantage of AM is the design freedom that is illustrated in the study conducted by Bacellar *et al*. [41]. The scholars investigate the design freedom of AM in air-to-fluid cross flow heat exchangers. In a conventional air-to-fluid cross flow heat exchanger, alteration of the fins is used to enhance heat transfer. The scholars argue that with the modern manufacturing capabilities of AM, the tube geometry should be investigated to enhance the performance instead of the fins. In ensuing Figure 2-10, the conventional heat exchanger and the newly adapted version are illustrated.

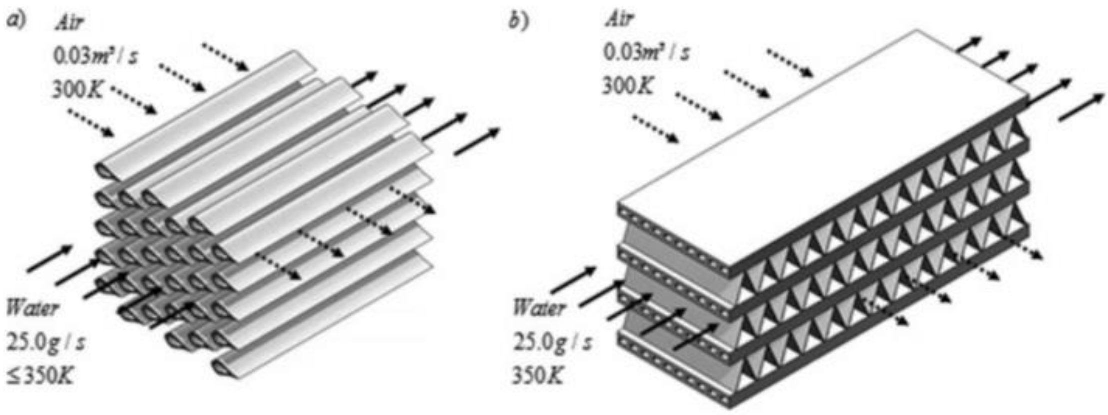

Figure 2-10: a) Finless heat exchanger b) baseline air-to-fluid heat exchanger[41]**.**

The objectives of the study are to numerically illustrate that when the fins become inefficient at smaller characteristic lengths, the need for a finless heat exchanger arises. The study opts to design a 1kW air-to-water heat exchanger and compare it to a state-of-the-art Micro heat exchanger. Consequently, it presents a proof of concept design that utilises a finless tube to ultimately provide a comprehensive analysis and shape optimisation approach to enhance the proof of concept design through CFD. The study reveals that the finless heat exchanger had a reduction of 20% in size, 20% reduction in air pressure drop, 40% reduction in material volume and an increase in heat transfer of 39% [1], [34].

The design freedom is also investigated by Bernardin *et al.* [22] in enhancing a traditional shell-and-tube heat exchanger with additively manufactured twisted tubes. The study selects a rounded rectangular tube shape and twisted it with a pitch of 41.3mm as illustrated in ensuing Figure 2-11.

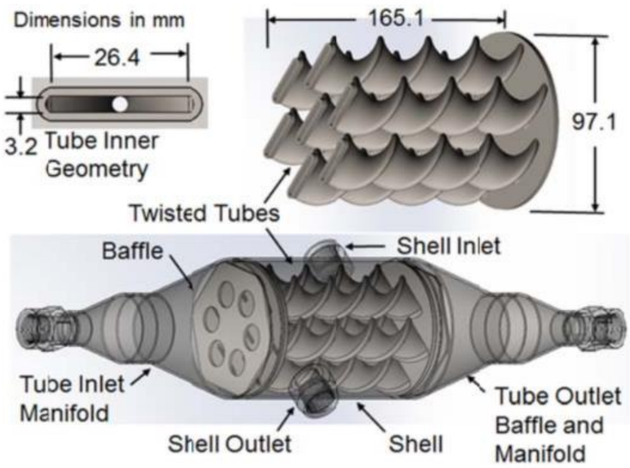

Figure 2-11: Bernadin et al.'s[22] **study on shell-and-tube heat exchanger with AM twisted tubes.**

The study selects for the pitch in this manner to ensure that the overhang would not exceed 40 degrees from the horizontal plain. The reason for this is that during AM, support structures are necessitated when the geometry has an overhang larger than 40 degrees from the horizontal plain. As a consequence, the support structure has to be machined away in the post processing stage, which results in extra cost in material and manufacturing time. A CFD study is conducted to illustrate the benefits that a complex geometry may offer over the traditional manufacturing methods. Similarly, the CFD is utilised as a verification and validation for the enhancements that AM could provide. The twisted tube heat exchanger illustrates an increase of 40% in the overall heat transfer coefficient accompanied with an increase in the internal pressure drop of 37% [22].

The HCFT-HX investigated in this study is manufactured by Extek and the composition of the Titanium used to fabricate the heat exchanger is not explicitly stated, therefore, it is assumed to be pure grade titanium [42]. Titanium also has a strong resistance against corrosion and fouling, and as stated in Chapter 1, the HCFT-HX operates in testing conditions where corrosion is actively present [6]. The heat exchanger is initially manufactured out of copper, however, owing to the pH of the process water, titanium is used as a replacement for its corrosion resistance.

As stated in Chapter 1, titanium is known as a hard and lightweight material, with the strength of steel with 60% of its density [43]. This characteristic makes it difficult to machine through traditional manufacturing techniques. Additionally, the cutting and removing of material through traditional manufacturing process result in wastage. Hence, the manufacturing of Titanium through employing AM may be a viable alternative [43]. Manufacturing commercially pure titanium through AM is feasible, however, the most commonly used titanium in the AM industry is the alloy Ti64 [44].

Concluding the literature study, it demonstrates that AM has the ability to manufacture and enhance heat exchangers. The design freedom that AM offers also breaks the barriers that were inflicted by traditional manufacturing, presenting an innovative perspective of enhancing heat exchangers.

CHAPTER 3: MODEL DEVELOPMENT

This chapter will provide a brief background of the basic thermodynamic theory and CFD principles used to resolve complex flow challenges; particularly the flow in HCFT-HX. In addition to this it *will comprise the steps taken to accurately model the HCFT-HX. A descriptive section on the geometry and its aspects will be discussed.*

In the early twentieth century, research with respect to fluid dynamics were predominantly based on experimental and analytical procedures [45]. As computational power evolved in the late 20th century, CFD was developed [46]. CFD is based on the Navier-Stoke equations that describe how velocity, temperature, pressure and density relate to one another by employing numerical analysis, data structures and computational software to analyse fluid flow. When compared to experimental and theoretical procedures, CFD provides an advantage in universality, flexibility, accuracy and cost [22], [47], [48].

This study utilises STAR-CCM+ as the CFD software to simulate the HCFT-HX. This chapter provides a detailed discussion of the selection process on the three categories that effect the simulation's accuracy, namely; mesh, physics and geometry. In Figure 3-1 below the layout of this chapter is illustrated;

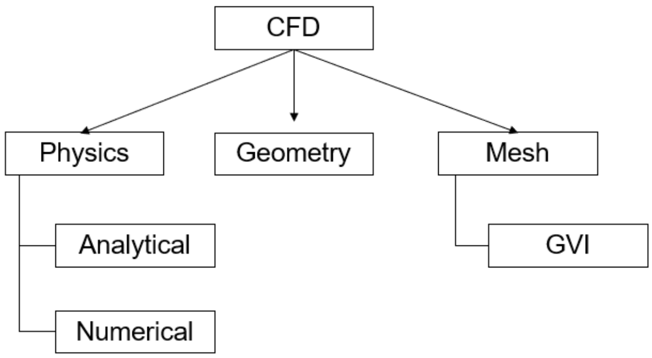

Figure 3-1: Chapter outline [own creation]

As a result, the chapter explores the theory of the analytical and numerical physics utilised in this study. The physics and mesh component of the HCFT-HX simulation are structured with the support of literature.

3.1 Physics

The selection of the physics model in CFD is critical as it determines the particle flow and how the governing equations are solved. In the following sections the basics of heat transfer are discussed and how the physics model is selected for the simulation of the HCFT-HX.

3.1.1 Physics: Analytical

As highlighted in the literature review, multiple engineering practices operate in the turbulent region [16], [23], [25], [49], [50]. The basic definition of turbulence is defined in 1937 by Von Karman as "…an irregular motion which in general makes its appearance in fluids, gaseous or liquid, when they flow past solid surfaces or even when neighbouring streams of the same fluid flow past or over one another" [51]. The basic physics of any thermal dynamic calculation, turbulent or laminar, comprise the following three continuity equations;

1. **Conservation of mass** - stating that the rate of mass entering the system is equal to the rate of mass exiting the system with the additional accumulation of mass within the system [47].

$$\frac{D\rho}{Dt} + \rho\nabla.\bar{v} = 0 \qquad \textbf{[3-1]}$$

   Where ρ is the fluid density, t is time and $\bar{v}$ is the flow velocity vector field.

2. **Conservation of momentum** - also known as the Navier-Stokes equations. The ensuing three equations are based on Newton's second law of motion "The momentum of an object is proportional to the net force that is acting on it in the same direction" [48]. The net force that is subjected to the body is gravitation and surface forces [47]. These three equations represent Newton's second law of motion in the directions of the cartesian coordinate system.

$$\rho\left(\frac{\partial u}{\partial t} + u\frac{\partial u}{\partial x} + v\frac{\partial u}{\partial y} + w\frac{\partial u}{\partial z}\right) = \rho g_x - \frac{\partial \rho}{\partial x} + \mu[\frac{\partial^2 u}{\partial x^2} + \frac{\partial^2 u}{\partial y^2} + \frac{\partial^2 u}{\partial z^2}] \text{ (x-direction)} \qquad \textbf{[3-2]}$$

$$\rho\left(\frac{\partial v}{\partial t} + u\frac{\partial v}{\partial x} + v\frac{\partial v}{\partial y} + w\frac{\partial v}{\partial z}\right) = \rho g_y - \frac{\partial \rho}{\partial y} + \mu[\frac{\partial^2 v}{\partial x^2} + \frac{\partial^2 v}{\partial y^2} + \frac{\partial^2 v}{\partial z^2}] \text{ (y-direction)} \qquad \textbf{[3-3]}$$

$$\rho\left(\frac{\partial w}{\partial t} + u\frac{\partial w}{\partial x} + v\frac{\partial w}{\partial y} + w\frac{\partial w}{\partial z}\right) = \rho g_z - \frac{\partial \rho}{\partial z} + \mu[\frac{\partial^2 w}{\partial x^2} + \frac{\partial^2 w}{\partial y^2} + \frac{\partial^2 w}{\partial z^2}] \text{ (z-direction)} \qquad \textbf{[3-4]}$$

With g_x , g_y, g_z the body's gravitational forces in the three directions, μ the fluid's viscosity, p the static pressure and u, v and w the velocity components.

3. **Conservation of energy** - where the first law of thermodynamics states that energy cannot be created nor destroyed, however, it can be transformed from one form to another.

$$\frac{d\boldsymbol{E}}{d\boldsymbol{t}} = \dot{\boldsymbol{Q}} + \dot{\boldsymbol{W}} \qquad \textbf{[3-5]}$$

Equation [3-5] may be described as the internal energy and kinetic energy ($\frac{dE}{dt}$) equal to the rate of energy transported by heat transfer ($\dot{Q}$) and the net rate of work ($\dot{W}$) done on the control volume (CV) by its surroundings as illustrated by Figure 3-2 [52].

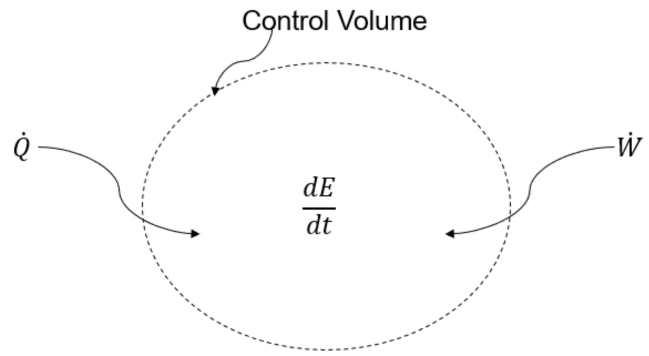

Figure 3-2: Control volume schematic [own creation]

Bergman *et al*. [52] indicate that heat transfer comprises three modes, namely; conduction, convection and radiation, however, for the purpose of this study radiation heat transfer will not be discussed, since the effect of radiation inside the heat exchanger is negligible.

The definition of heat transfer is given as the thermal energy in transit owing to a spatial temperature difference [52]. When a temperature gradient exists in a stationary medium (solid or fluid) the term conduction is used to refer to the heat transfer that will occur across the stationary medium. In contrast, the term convection refers to heat transfer that will occur when a temperature difference is present between a surface and a moving fluid [52].

Heat transfer processes may be quantified in terms of rate equations, where the amount of energy in transit is computed per unit time. For heat conduction the rate equation is;

$$q_x'' = -k\frac{dT}{dx} \quad \textbf{[3-6]}$$

Where the heat flux q_x'' is the heat transfer rate in the x-direction per unit area perpendicular to the direction of transfer and is proportional to the temperature gradient $\frac{dT}{dx}$. The parameter k is a transport property of the medium through which the energy is moving and is also known as the thermal conductivity. In steady state conditions where a wall thickness of L and thermal conductivity of k are identified, the heat flux through the wall may be described with equation [3-7] and Figure 3-3Figure 3-3: Thermal conduction illustration [52];

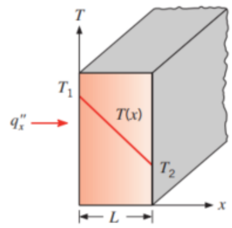

Figure 3-3: Thermal conduction illustration [52]

$$q_x'' = -k\frac{T_2 - T_1}{L} \quad \textbf{[3-7]}$$

In steady state convection, the heat flux from the surface to the fluid is described in equation [3-8] and Figure 3-4 with surface temperature T_s, ambient temperature of T_∞ and a moving fluid with a convection heat transfer of coefficient h. The heat transfer coefficient is a characteristic parameter of the fluid that is dependable on the surface geometry, nature of the fluid motion and the fluid's thermodynamic and transport properties [52], [53].

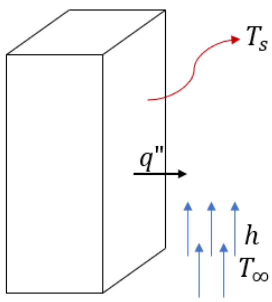

Figure 3-4: Heat flux for convection [own creation]

$$q'' = h(T_s - T_\infty) \quad \textbf{[3-8]}$$

With regards to cylindrical coordinate system, the conduction heat transfer rate is as illustrated in equation [3-9] and Figure 3-5;

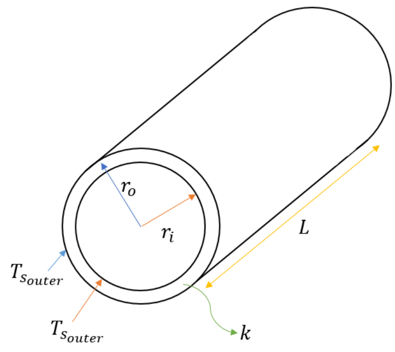

Figure 3-5: Cylindrical illustration of conduction

$$q_{conduction} = 2\pi Lk\left(\frac{T_{s_{outer}} - T_{s_{inner}}}{ln\left(\frac{r_o}{r_i}\right)}\right) \quad \textbf{[3-9]}$$

For the convection heat transfer rate in a cylindrical system, it is illustrated by equation [3-10] and Figure 3-6;

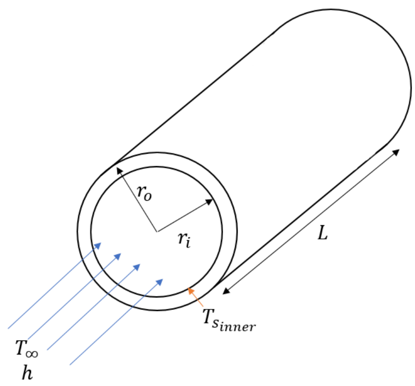

Figure 3-6; Cylindrical illustration for convection

$$q_{convection} = 2\pi r_i Lh(T_{s_{inner}} - T_\infty) \quad \textbf{[3-10]}$$

With r_i and r_o the inner and outer radius of the cylindrical tube respectively, L the length of the tube, $T_{s_{inner}}$ and $T_{s_{outer}}$ the internal and external surface temperature of the pipe respectively, T_∞ the ambient temperature of the fluid, k the thermal conductivity of the pipe and h the average convection heat transfer coefficient.

The heat transfer coefficient is obtained by the following equation;

$$\boldsymbol{Nu = \frac{h\,D_h}{k}} \qquad \textbf{[3-11]}$$

$$\boldsymbol{D_h = \frac{4A}{P}} \qquad \textbf{[3-12]}$$

With the Nusselt number expressed as Nu and the hydraulic diameter as D_h that is defined by equation [3-12] above, with A the cross-sectional area of the pipe and P the wetted perimeter of the duct. The Nusselt number is a dimensionless number, and is defined as the ratio of convection heat transfer over conduction heat transfer at a boundary of a fluid [52], [53].

The Nusselt number is often used to quantify heat transfer enhancements on heat exchangers. In enhancing a heat exchanger, multiple techniques exist and are classified as passive, active or compound enhancement techniques [18]. Passive techniques are described as alterations to the geometry, surface roughness and/or material, where active techniques require direct application of an external electrical source to enhance the heat transfer [54], [55]. The compound technique is the application of both active and passive techniques.

Passive techniques may be described consideration equation [3-10], where the thermal energy transported through convection is described. This equation illustrates that the amount of thermal energy transported is directly proportional to the contact surface area between the fluid and the duct. By enlarging the contact surface area, the thermal energy will increase. In practise, this is accomplished using flute or flutes. The HCFT-HX utilises the fluted tube geometry to increase the contact surface between the water and pipe. The HCFT-HX comprises a super-heated refrigerant flowing in the outer annulus, while water flows in the inner fluted tube as illustrated in Figure 3-7 below.

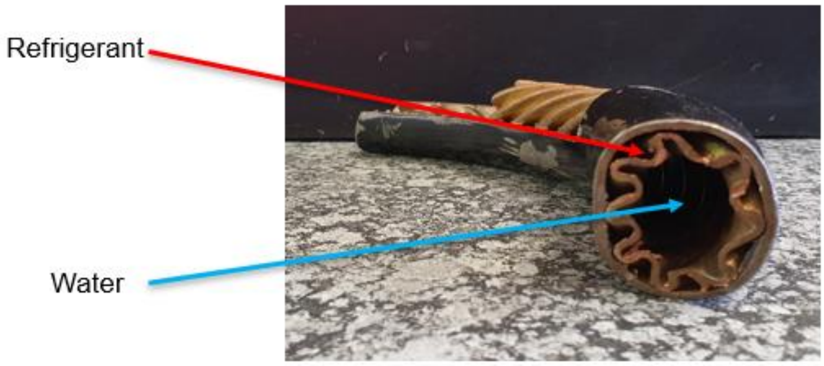

Figure 3-7: Flow illustration

Simulating both the super-heated refrigerant and the internal fluid is computationally expensive as the super-heated refrigerant undergoes two-phase flow and is not within the scope of this study. Therefore, the heat transferred from the super-heated refrigerant to the water is calculated with equation 3-13 (described below) and applied to the fluted tube.

$$\boldsymbol{q = \dot{m}c_p(T_{w_o} - T_{w_i})} \qquad \textbf{[3-13]}$$

This study assumes that the internal fluid is incompressible flow and modelled in the steady state time domain, therefore, this equation may be used. With $\dot{m}$ the mass flow of the fluid, c_p the average specific heat capacity for the fluid at the average temperature and pressure of the pipe. The thermal energy obtained from [3-13] will then applied to the outer surface of the inner fluted tube.

3.1.2 Physics: Numerical Method

Since the start of the twentieth century, the task to determine the ideal turbulent model in CFD has been a challenge, owing to the characteristics of turbulent flow [56]. Although the basics of heat transfer are still applied in CFD, a second order partial derivative is used to solve more complex equations that describe particle turbulent flow. To accurately capture the particle flow, the correct space, time and motion models should be selected, namely;

i. Space correlates to the mesh that is be discussed in the following section.
ii. Time correlates to the steady state or transient state for the internal fluid, this study will employ steady state.
iii. Motion refers to the turbulence models which a wide selection is provided for in STAR-CCM+ as illustrated in ensuing Figure 3-8 .

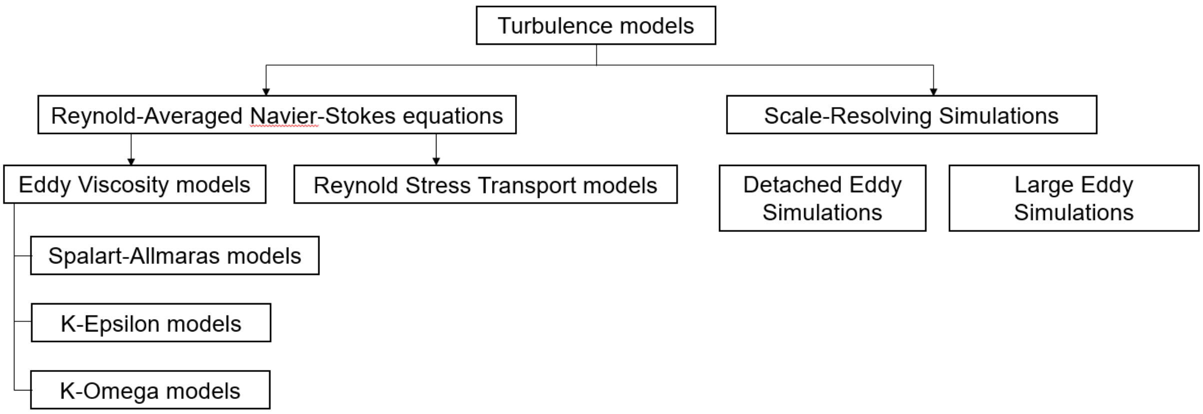

Figure 3-8: STAR-CCM+ Turbulence models

Sodja *et al*. [57] affirm that turbulence flow is complex in nature, since turbulence dominates all other forms of flow, necessitating a contemporary approach to correctly model turbulence. The complexity of simulating turbulent flow is due to the Navier-Stokes equations described in equation [3-2] to [3-4]. The Navier Stokes equations are inherently a nonlinear and three-dimensional partial differential equation.

The difficulty in simulating turbulence is that one strives to model a complex phenomenon with a model as simple as possible [57]. As a result, the models based on the Reynold-Average Navier-Stokes (RANS) equations are appropriate to use for simulating turbulent flow as it is less computational expensive when compared to its counterparts [58].

As previously stated, the RANS models are based on the Navier-Stokes equations described in equations [3.2]-[3.4] with the additional term of the Reynold stress tensor $\bar{\tau}_{ij}$ described below.

$$\bar{\boldsymbol{\tau}}_{ij} = -\boldsymbol{\rho}\begin{pmatrix} \overline{u'u'} & \overline{u'v'} & \overline{u'w'} \\ \overline{u'v'} & \overline{v'v'} & \overline{v'w'} \\ \overline{u'w'} & \overline{v'w'} & \overline{w'w'} \end{pmatrix} \textbf{[3-14]}$$

As illustrated in the preceding Figure 3-7, the RANS equations comprise a variety of turbulence models. The employment of these models as provided by the STAR-CCM+ user guide is listed as follow;

- **Spallart-Allmaras models -** are suited for the external flow in aerospace applications.
- **Reynold Stress Transport models -** most complex and computationally expensive models. These models are recommended for turbulent flow that is highly anisotropic such as the flow in a cyclone separator.
- **K-Epsilon models -** comprise a two-equation model that solves the turbulent kinetic energy k_t and the turbulent dissipation rate ϵ in order to determine the turbulent eddy viscosity μ_t.

$$\boldsymbol{\mu_t = \rho C_\mu \frac{k_t^2}{\epsilon}} \textbf{ [3-15]}$$

$$\boldsymbol{\epsilon = 2\left[\left(\frac{\partial u}{\partial x}\right)^2 + \left(\frac{\partial v}{\partial y}\right)^2 + \left(\frac{\partial w}{\partial z}\right)^2\right] + \left(\frac{\partial u}{\partial y} + \frac{\partial v}{\partial x}\right)^2 + \left(\frac{\partial v}{\partial z} + \frac{\partial w}{\partial y}\right)^2 + \left(\frac{\partial w}{\partial x} + \frac{\partial u}{\partial z}\right)^2} \textbf{ [3-16]}$$

The K-Epsilon models provide an acceptable compromise between robustness, accuracy and computational cost. According to the user guide of STAR-CCM+ [58], it is adequately suited for flow that contains complex recirculation with or without heat transfer. According to literature [47] conducted on CFD modelling of heat exchangers, the recommended K-Epsilon model is the “Realizable Two-Layer” model with the “All y+ Wall Treatment”.

Similar to the K-Epsilon models, the K-Omega models also solve two transport equations. Both of these models solve the turbulent kinetic energy k_t, however, they differ as the K-Omega models solve the specific dissipation rate ω in order to determine the turbulent eddy viscosity ϵ. One advantage that the K-Omega models have over the K-Epsilon models is its utilisation without requiring the computational wall distance. The disadvantage the K-Omega models with regard to the K-Epsilon models is that boundary layer computations are sensitive for the ω values in the free stream. This translates into extreme sensitivity in the inlet boundary conditions for internal flow. The K-Omega models are recommended for aerospace situation with external flow where near wall computations are required. Literature seldom provides any clear motive for selecting a specific turbulent model. Nonetheless, published studies predominately apply the K-Epsilon models [16], [17], [19], [20].

In order to ensure that the K-Epsilon model is the correct model to simulate heat transfer with turbulent flow, a smooth pipe's outlet temperature, Nusselt number and pressure drop are calculated and compared by means of Engineering Equation Solver (EES) and CFD.

3.1.3 Smooth tube verification

By ensuring that literature [16], [17], [19], [20] employed the correct physics model, two models (K-Epsilon and K-Omega) recommended by Siemens are compared to an analytical simulation [58]. EES is used for the analytical model, considering that the simulation comprises a simplified tube with internal flow and heat flux applied to the outer wall (illustrated in Figure 3-9 below). The simplified tube model is solved in EES and simulated in CFD to compare the results in making an informed decision

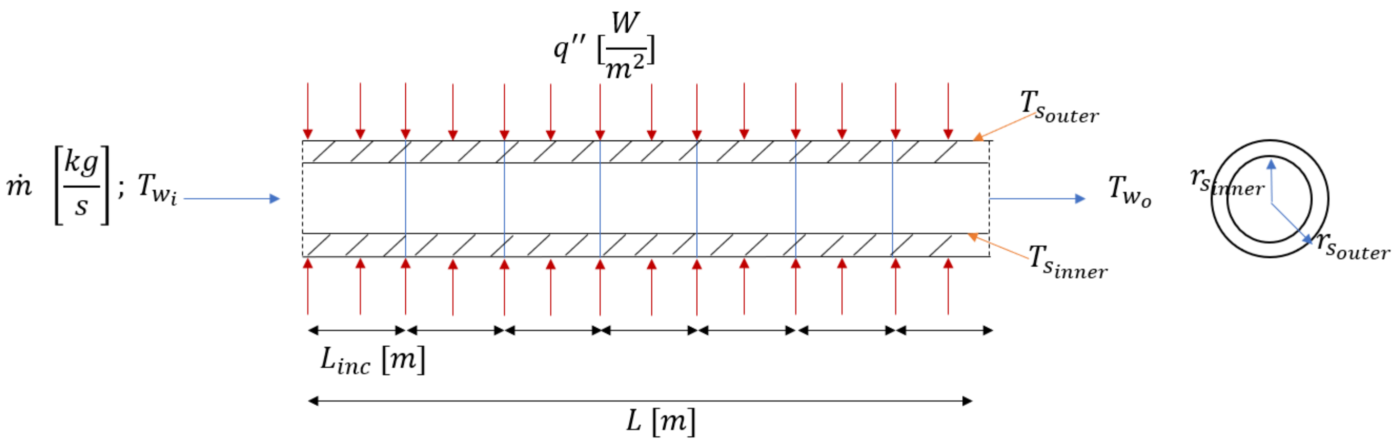

Figure 3-9:Schematic sketch of internal flow and heat flux. [own creation]

The physics in EES are solved per length increment (L_{inc}) of the pipe as illustrated in Figure 3-9 above. As previously stated, the heat transfer equations that describe the flow of thermal energy is the conduction equation [3-8] and the convection equation [3-10]. The flow of thermal energy per increment is illustrated in Figure 3-10 below with a thermal resistance diagram.

$$q[W] = q''[\frac{W}{m^2}] \times A_{outer_{surface}}[m^2]$$

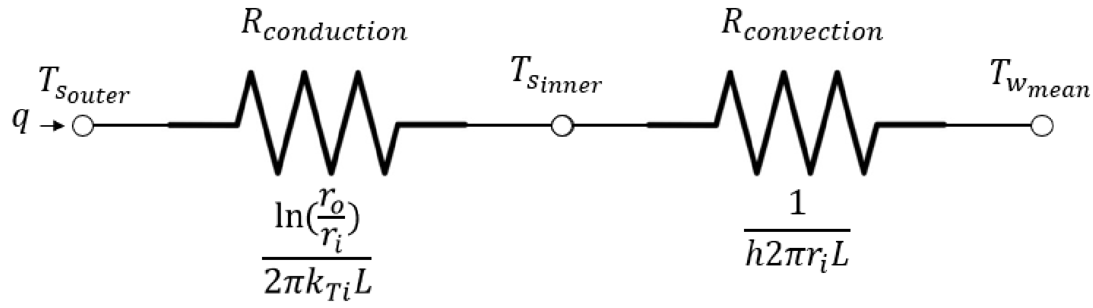

Figure 3-10:Thermal resistance schematic

- T_{o_s} and T_{i_s} represent the surface temperature of the outer wall and inner wall respectively.
- $T_{w_{mean}}$ is the average temperature of the water per increment and determined by the logarithmic equation 3-17 described below.

$$\frac{\left(\left(T_{s_{inner}} - T_{w_o}\right) - \left(T_{s_{inner}} - T_{w_i}\right)\right)}{\ln\left(\frac{T_{s_{inner}} - T_{w_o}}{T_{s_{inner}} - T_{w_i}}\right)} \quad \textbf{[3-17]}$$

- r_o and r_i present the outer and inner radius of the pipe respectively.
- $A_{outer_{surface}} = 2\pi r_o L$ is considered as the outer surface area of the pipe and
- k_{Ti} and h are considered as the thermal conductivity of the pipe material and the convection coefficient on the water side, respectively.

The results analysed are the outlet temperature of the fluid, the Nusselt number and the pressure drop over the pipe. The outlet temperature of the fluid is determined by solving the heat transfer equations, namely;

$$\boldsymbol{q = \dot{m}cp(T_{w_o} - T_{w_i})} \quad \textbf{[3-18]}$$

$$\boldsymbol{q_{convection} = hA_{inner} \frac{\left(\left(T_{s_{inner}} - T_{w_o}\right) - \left(T_{s_{inner}} - T_{w_i}\right)\right)}{\ln\left(\frac{T_{s_{inner}} - T_{w_o}}{T_{s_{inner}} - T_{w_i}}\right)}} \quad \textbf{[3-19]}$$

$$\boldsymbol{q_{conduction} = 2\pi Lk \left(\frac{T_{s_{outer}} - T_{s_{inner}}}{ln\left(\frac{\frac{D_o}{2}}{\frac{D_i}{2}}\right)}\right)} \quad \textbf{[3-20]}$$

$$q'' \times A_{outer_{surface}} = q = q_{conduction} = q_{convection} \quad \textbf{[3-21]}$$

With 15 variables consisting of 3 unknowns and 4 equations, the outlet temperature per increment is easily determined. The pressure drop is calculated with the aid of the Darcy Weisbach equation described in equation [3-22].

$$\Delta P = \frac{f \times \rho \times v^2 \times L}{2D_i} \quad \textbf{[3-22]}$$

- With ΔP the pressure drop,
- f the Darcy friction factor,
- D_i the inner diameter of the pipe.

The full calculations of the model developed in EES are listed in ANNEXURES. The physics models for the CFD and their subcategory models used in determining the best suited physics model are listed in Table 3-1 below.

Table 3-1: CFD Physics selection

Parameter		**Reason**
Fluid Physics		
Space	Three-dimensional	To capture the particle flow in the x, y and z direction.
Time	Steady	The study assumes steady state in the heat exchanger.
Material	Liquid > Water	The fluid in the HCFT-HX is water therefore water may be selected in this model as well.
Flow type	Segregated	Segregated flow is recommended for internal flows.
Equation state	Constant density	A constant density is assumed as no boiling is present in the HCFT-HX.
Viscous Regime	Turbulent> RANS > **K-Epsilon/Omega**	According to literature the K-Epsilon model is constantly used and to assure this is the correct model the user guides other recommended model will be used.

Solid Physics		
Space	Three-dimensional	The solid and fluid model have to be the same dimension
Time	Steady	The pipe is stationary and solid, thus steady state may be selected.
Material	Solid > Titanium (considered pure)	This is the material used in the HCFT-HX
Optional	Segregated Solid Energy	To apply a heat source on the outer wall of the pipe this model has to be selected.
Equation state	Constant density	The study assumes constant density of the solid.

A detailed description of the mesh selection for the HCFT-HX will be discussed in Chapter 3.3. A standard mesh comprising a y+ value less than 5 is selected for the smooth tube simulation. The simulation model is constructed with a basic polyhedral mesh of 3mm base size and 3 prism layers in a 0.4mm thickness as illustrated in Figure 3-11 below.

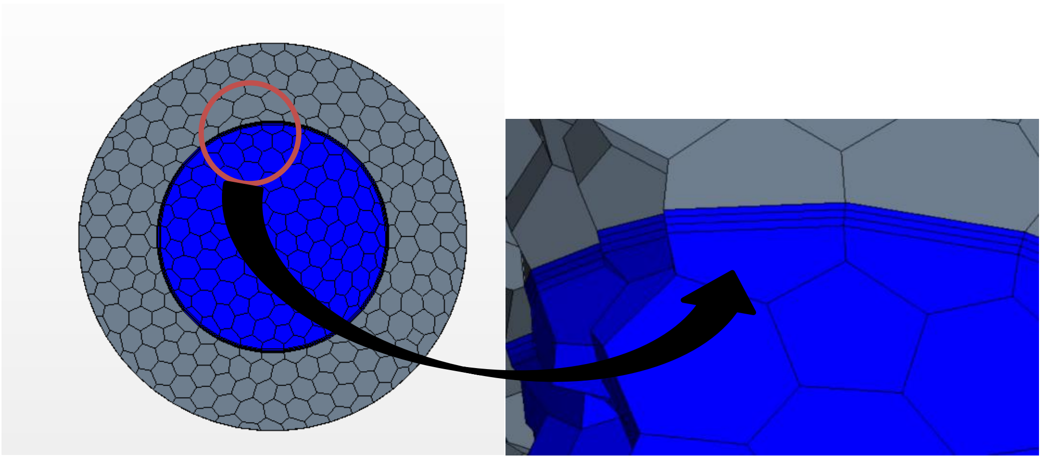

Figure 3-11: Illustration of mesh for smooth tube

The input values of the verification of the physics model are selected as illustrated in Table 3-2 below.

Table 3-2: Inputs for verification

Parameter	Value	Unit
Heat flux	10 000	W/m^2
Mass flow of water	0.09	kg/s
Inlet temperature	20	℃
Length of tube	1000	mm
Inner Diameter	30	mm
Outer diameter	50	mm
Material	$Titanium\ (Pure)$	$-$

The EES model is based on the fundamentals of heat transfer, therefore, in ensuring the fundamentals of this study are accurate, the EES results are classified as theoretical results. The results of the EES code and CFD simulation are illustrated in Table 3-3. The percentage error in Table 3-3 is determined by equation [3-23].

$$\%\boldsymbol{error} = \frac{\boldsymbol{Theoretical - Simmulated}}{\boldsymbol{Theoretical}} \qquad \textbf{error} \quad \textbf{[3-23]}$$

Table 3-3: EES and CFD Results

EES		**CFD**			
		K-Epsilon	**%error**	**K-Omega**	**%error**
Temperature difference [C]	4.17	4.16491	0.122062%	4.15847	0.276499%
Pressure drop [Pa]	14.8796	14.47447	2.72319%	11.7151	21.267%
Nusselt number	37.38	37.28615	2.84467%	29.41267	21.314%

For the Nusselt numbers, the EES value is calculated using equation [3-8]. The CFD's Nusselt number value is determined with STAR-CCM+'s built-in Nusselt number function that is based on equation [3-11]. The built-in Nusselt numbers function is described in equation [3-24].

$$\boldsymbol{Nu} = \frac{\dot{q}''_{wall} \times L_{ref}}{(T_{ref} - T_{wall}) \times k_{ref}} \qquad \textbf{[3-24]}$$

With $\dot{q}''_{wall}$ the wall heat flux, k_{ref} the thermal conductivity reference value, L_{ref} the reference length, T_{ref} the reference temperature and T_{wall} the temperature at the wall. The reference values, with regards to the internal flow of the pipe, are selected as follow;

- L_{ref} is die inner diameter of the pipe,
- T_{ref} the inlet temperature of the fluid,
- k_{ref} the thermal conductivity of the fluid at interface.

As noted in Table 3-3, the K-Epsilon has a %error value for less than 5% and is the most accurate in representing the analytical value of internal turbulent flow. The difference in values may be subjected to the CFD computing the values in a 3D coordinate system whereas EES only calculates in a one-dimensional coordinate system. Together with this, the two systems have different solving strategies values.

The solving strategy of EES is discretising the full length of the pipe into smaller sections/increments. To ensure the discretisation is sufficient, the number of increments are altered and the results are observed. As illustrated in Figure 3-12, the number of increments are sufficient.

1..10	n	$T_{w;final}$	$pressure_{drop}$	k_{avg}	h_{avg}
Run 1	3	24,172368	14,8799062	0,6016	749,6
Run 2	9	24,172364	14,8795995	0,6016	749,6
Run 3	12	24,172363	14,8795819	0,6016	749,6
Run 4	15	24,172363	14,8795739	0,6016	749,6
Run 5	1	24,172406	14,8823288	0,6016	749,7
Run 6	21	24,172363	14,8795669	0,6016	749,6
Run 7	24	24,172363	14,8795653	0,6016	749,6
Run 8	27	24,172363	14,8795642	0,6016	749,6
Run 9	30	24,172363	14,8795635	0,6016	749,6
Run 10	33	24,172363	14,8795630	0,6016	749,6

Figure 3-12:EES discretization

Considering that CFD solves the problem iteratively, a guess value is provided in CFD and the deference between the guess value and the calculated value is identified as the residuals. The residuals are a fundamental measurement of an iterative solution's convergence that directly quantifies the error in the solution of the system of equations. In an iterative numerical solution (as in a CFD simulation), the residual will never be exactly zero, however, the lower the residual value, the more numerically accurate the solution will be. A value of less than 1E-3 is considered to be roughly accurate and values of 1E-5 is considered to be accurate [46], [47], [59]. The residual monitor plot of the CFD simulation is illustrated in Figure 3-13.

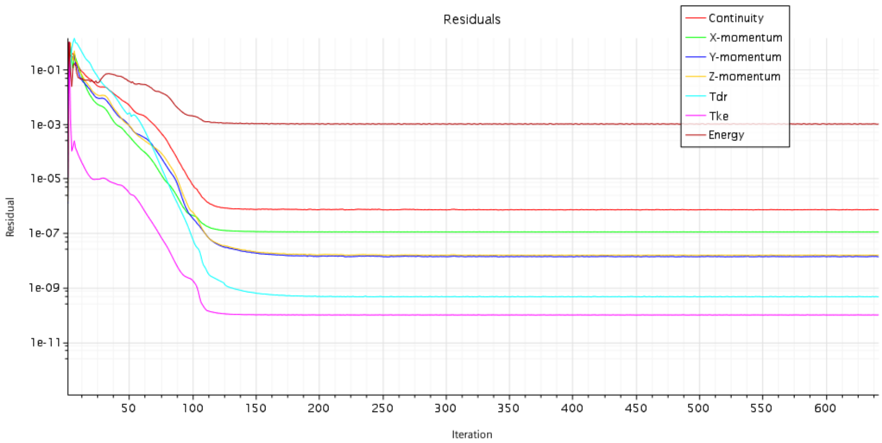

Figure 3-13: Residual monitor plot

Knowing that the results are converged and stable, it may be concluded that the K-epsilon model is the correct physics model to simulate internal turbulent flow with a %error of less than 5%. Therefore, it may be assumed that the HCFT-HX may be simulated with the same physics model.

3.2 Geometry

The geometry utilised in CFD is constructed in a Computer Aided Design (CAD) software and saved as a STL file. The format in which the file is saved is termed stereolithography file. In this format the shape is tessellated into triangles. CFD is used to simulate real-life problems, therefore, the geometry of the simulation model should replicate the real-life phenomenon. The process of determining the model's geometry of the HCFT-HX is discussed in ensuing chapter 3.2.1

3.2.1 HCFT-HX geometry verification

As indicated in the previous chapter, geometry is a vital component in accurately simulating a real-life phenomenon. The HCFT-HX's inner tube geometry is defined by two notable characteristics, namely; the cross-section and flute pitch. These characteristics are geometrically complex, owing to the difficulty in measuring. As a result, to create an accurate CAD model of the inner tube may be intimidating. Another characteristic of the HCFT-HX is the shape of the coiled pack, since it correlates to a trombone shape as illustrated in Figure 3-14 a) below. To accurately design the cross-section of the tube, an imprint was taken of the HCFT-HX as illustrated in Figure 3-14 b) below.

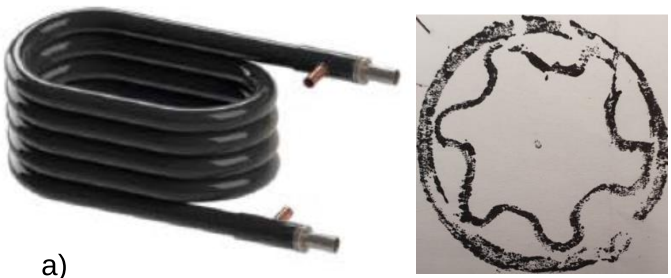

a) b)

Figure 3-14: Imprint taken from cross-sectional geometry of HCFT-HX.

In order to construct the model in CAD with the imprint, a photo is taken and imported into SolidWorks where the cross-sectional geometry could be traced to ensure accuracy. By determining the flute pitch, the length of full rotation is measured and inserted in the CAD through utilising a sweep rotation. In verifying the geometry's accuracy, the model is printed by means of Polymer AM and compared to a cut-off of the actual heat exchanger as illustrated in Figure 3-15 below.

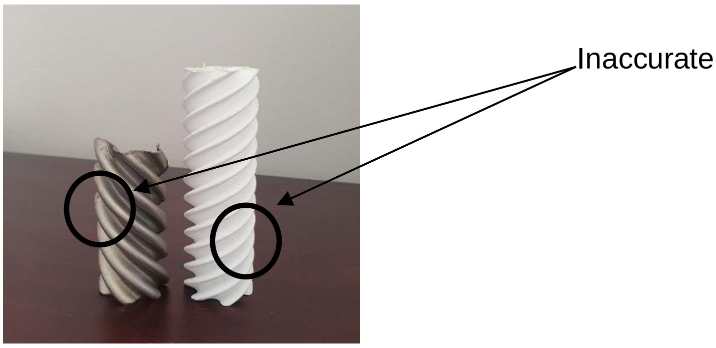

Figure 3-15: First iteration of CAD model

As noted in Figure 3-15, the CAD geometry does not resemble the actual cross-sectional form, as the flute's rounding are sharper when compared to the actual model. This resulted in a second iteration where only a single flute is traced and repeated in a circular pattern. The CAD model is subsequently printed and compared to the cut-off as presented in Figure 3-16 below. Noticeably, the second iteration's rounding of the flutes are representative of the cut-off. Given that the cross-sectional geometry and flute pitch are accurate and verified, a CAD model of the heat exchanger may be created.

Figure 3-16: Second iteration of CAD model.

As stated above, the HCFT-HX is a coiled trombone shape rather than a circular one and the dimensions of the actual heat exchanger's helical coil are measured and applied in CAD. The helical pack of the heat exchanger comprises 4.5 revolutions, however, a single revolution of the heat exchanger is created as the computational capacity is limited. The resulting CAD models are illustrated in Figure 3-17 below. Note that the entire heat exchanger is illustrated on the left (a) and the single revolution of the heat exchanger is illustrated on the right (b).

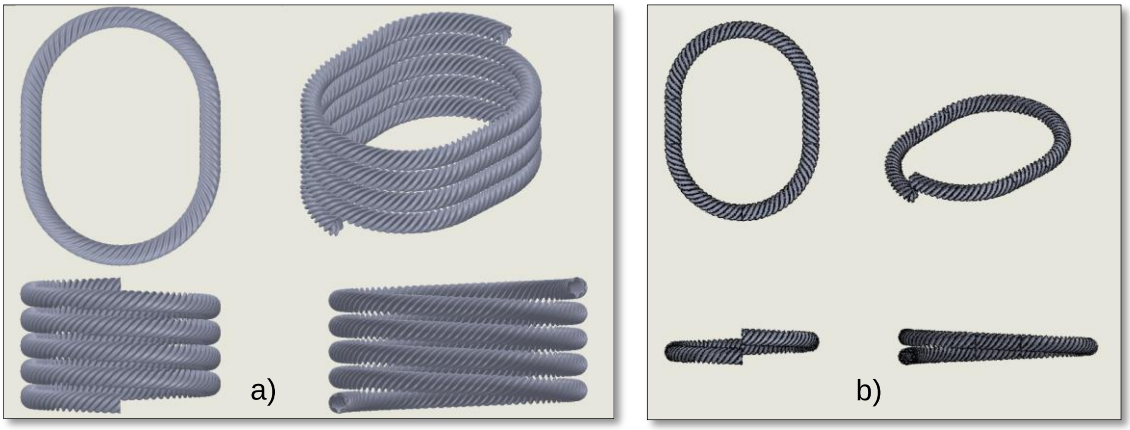

Figure 3-17: Entire heat exchanger model in CAD

With the finalisation of the CAD file, the dimensions of the heat exchanger may be accurately measured. An illustration of the dimensions is provided in Figure 3-18 and the dimensions are listed in Table 3-4.

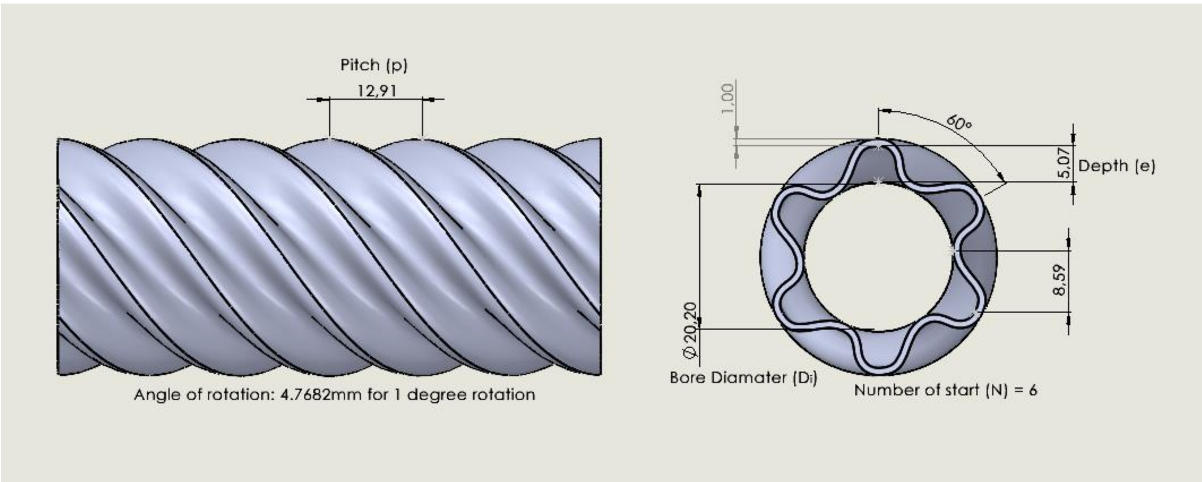

Figure 3-18: Descriptive illustration of dimensions.

Table 3-4: HCFT-HX dimensions.

Parameter	Value	Unit
Inner tube length	4 789.845	mm
Number starts	6	$-$
Flute pitch	12.91	mm
Flute depth	5.06	mm
Coil revolutions	4.5	$-$
Fluted tube wall thickness	0.7	mm
Coil Pack Height	180	mm
Coil Pack Length	372	mm
Coil Pack Width	280	mm

3.3 Mesh

Meshing is described as the discretisation of a geometric domain [58]. The mesh may be classified into two types, namely; a finite element (FE) mesh that computes values at the elemental node and a finite volume (FV) mesh that computes values at the cell centre. For the purpose of this study, a FV mesh is applicable due to the presence of flow. A FV mesh is constructed with the following entities as illustrated in Figure 3-19 below:

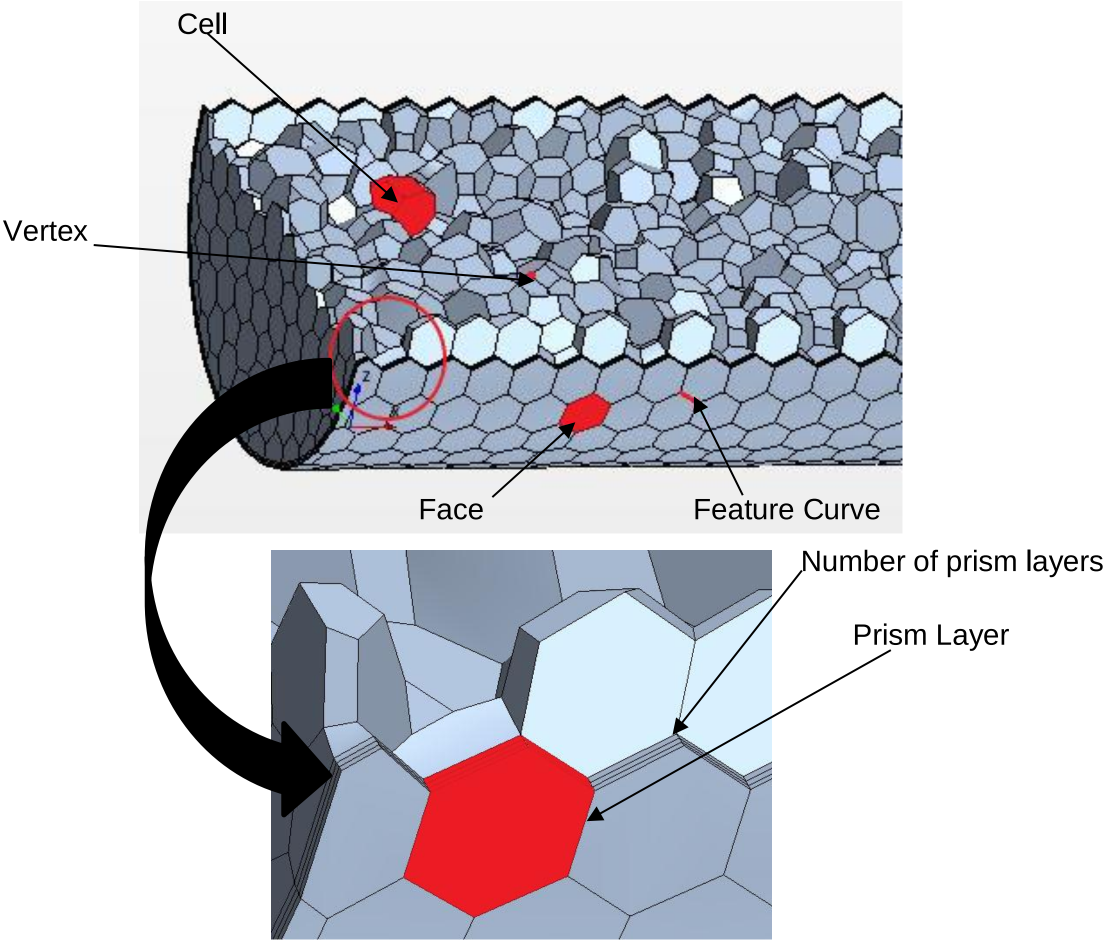

Figure 3-19: A mesh's basic components[58]**.**

- A Vertex is a point that is defined by a position vector and multiple vertices may be used to describe a face or feature curve.
- A Face comprises an ordered collection of vertices to define a surface in 3D space.
- Feature curves consist of two vertices and are represented by a line.
- The Cell is the ordered collection of faces to define a closed volume, representing a CV. The three-dimensional form of a cell can either be polyhedral (polyhedral mesh) or tetrahedral (tetrahedra mesh) as illustrated in Figure 3-1920. For the purpose of

complex flow, a polyhedral mesh is recommended as it is less computationally draining than its counterpart and provides similar accuracies with fewer cells [58].

- Prism Layer cells are a specialised cell that constructs the prism layer. The prism layer is generally in models that comprise near wall flow, for instance; internal flow in a pipe. Most models require a prism layer for accuracy. Moreover, the prism layer is constructed by a number of thin cells and the values that can be altered is the number of prism layer cells. The total thickness of the prism layer and the prism layer cell growth stretching.

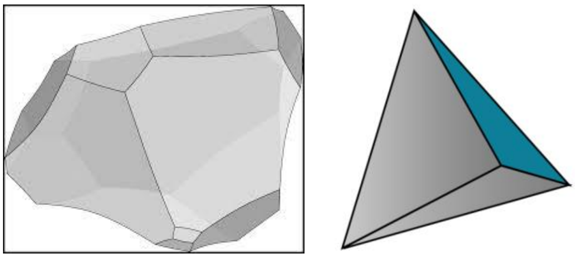

Figure 3-20: Polyhedral cell a) and Tetrahedral cell b)[60]

The polyhedral mesh used in STAR-CCM+ consists of reference values that influence the mesh's compositions, for instance; base size and stretching factors. The base size value represents the size on which the polyhedral cell is constructed that extensively determines the number of cells in the mesh. In regards to accuracy, the more cells (fineness of the mesh) employed in the model the greater the accuracy will be, however, there is a certain limit where the improved effect of the number of cells become redundant. To investigate the effect that the fineness of the mesh has on the accuracy of the output data, a Grid Verification Index (GVI) may be conducted and is extensively discussed in Chapter 3.3.2

The other important aspect of meshing is determining the correct wall treatment for the simulation and is explained in the following section.

3.3.1 Wall Treatments

The necessity of accurately predicting the flow and turbulence across walls are essential as they are a source of vorticity in multiple flow problems [58]. Three sublayers exist in the inner region of the boundary layer and may be modelled using empirical approaches. Figure 3-21: Three different sublayers in the inner boundary layer region with their accompanied y+ wall treatment [29]. illustrates these three sublayers with their accompanied dimensionless wall distance y+. The blue line in Figure 3-21 represents the equations for the velocity profile in a fully developed flow.

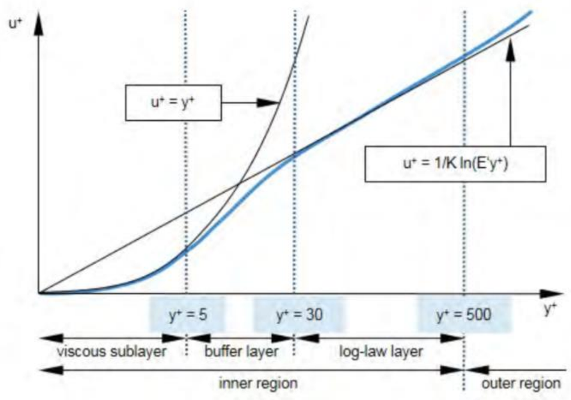

Figure 3-21: Three different sublayers in the inner boundary layer region with their accompanied y+ wall treatment [29].

The wall distance y+ is a dimensionless wall distance and is directionally proportional to the velocity profile as depicted in Figure 3-22.

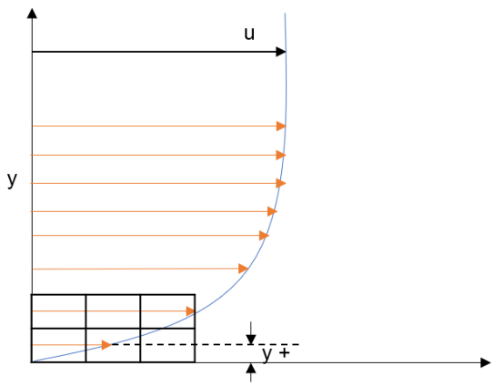

Figure 3-22: The velocity profile of turbulent flow and internal flow.

Three different empirical equations may be used to solve each of the three sublayers and are categorised according to their y+ value, for example;

1. For a low y+ comprising a value of 0< y+ <5, the sublayer falls in the viscous sublayer, and is represented by a linear line equation namely:

$$U^+ = y^+$$

The viscous sublayer is extremely computational draining as it requires a fine mesh with fine near wall cells (prism layers) to capture them.

2. For y+ having a value of 5< y+ <30, the sublayer categorises into the buffer sublayer. As depicted in Figure 3-21, the blue curve is the equation of how the velocity profile is represented. The two black lines represent the equations $U^+ = y^+$ and $U^+ = \frac{1}{K\ ln(Ey^+)}$. In the buffer sublayer, these two equations do not represent the blue line entirely, making this region unstable.
3. High y+ values comprise an y+ a value of y+< 30, in this region the log law equation is suitable for use. This sublayer's main advantage is that it requires less near wall cells and is able to predict accurately with a courser mesh.

In a study conducted by Shukla *et al.* [61], the effect of y+ values in curved pipes in the turbulent region is investigated. The study evaluates multiple physics models, including the K-Epsilon model, and determines that a lower y+ value provides enhanced results. The study identifies that a y+ value of $y{+}{<}\ 5$ provides more accurate readings. Similar studies recommend that a y+ value of less than 5 should be selected, as a result this study will utilise a y+ value of less than 5 [62], [63], [64]

3.3.2 HCFT-HX mesh verification

In order to obtain an accurate simulation of flow and heat transfer, an optimal quality mesh is necessitated. As deliberated in in the preceding section, the mesh is the discretisation of the CAD model, where the cells act as a CV and the physics are solved for each CV. Before the HCFT-HX may be simulated, the correct number of cells in the mesh should be selected. This is determined by initially selecting a coarse mesh and refining its base values until the results analysed have slight changes, this is referred to as a GVI. According to literature, the polyhedral volume mesh accompanied with the prism layer mesher are properly suited for internal flow [58]. To create a volume mesh, a surface mesh is initially created that requires a surface remesher. A surface remesher is employed to retriangulate a closed starting surface in improving the tessellation of the geometry. In the ensuing Figure 3-23 a surface mesh accompanied with its volume mesh are illustrated.

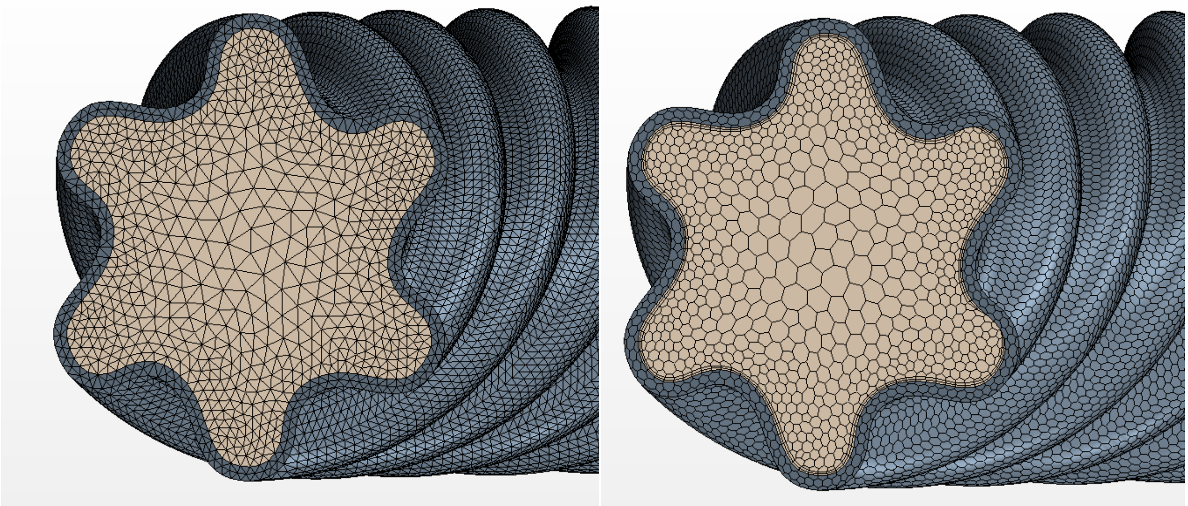

Figure 3-23: Surface mesh (left) and volume mesh (right)

Even though multiple parameters affect the number of cells in the model, the base size is considered to have the most significant effect. This study investigates the effect of the flute parameters on the heat exchanger's thermal performance, therefore, performing the GVI on the fluted tube with the largest depth may well provide a safety factor as this model will have the most complex curves. In Figure 3-24 below, the different meshes with alternating base values are illustrated. The stretching factor of 1.5 is selected to ensure that the flute's depths are meshed with a finer cell than in the centre. This assists by reducing a drastic change in prism layer and polyhedral cell.

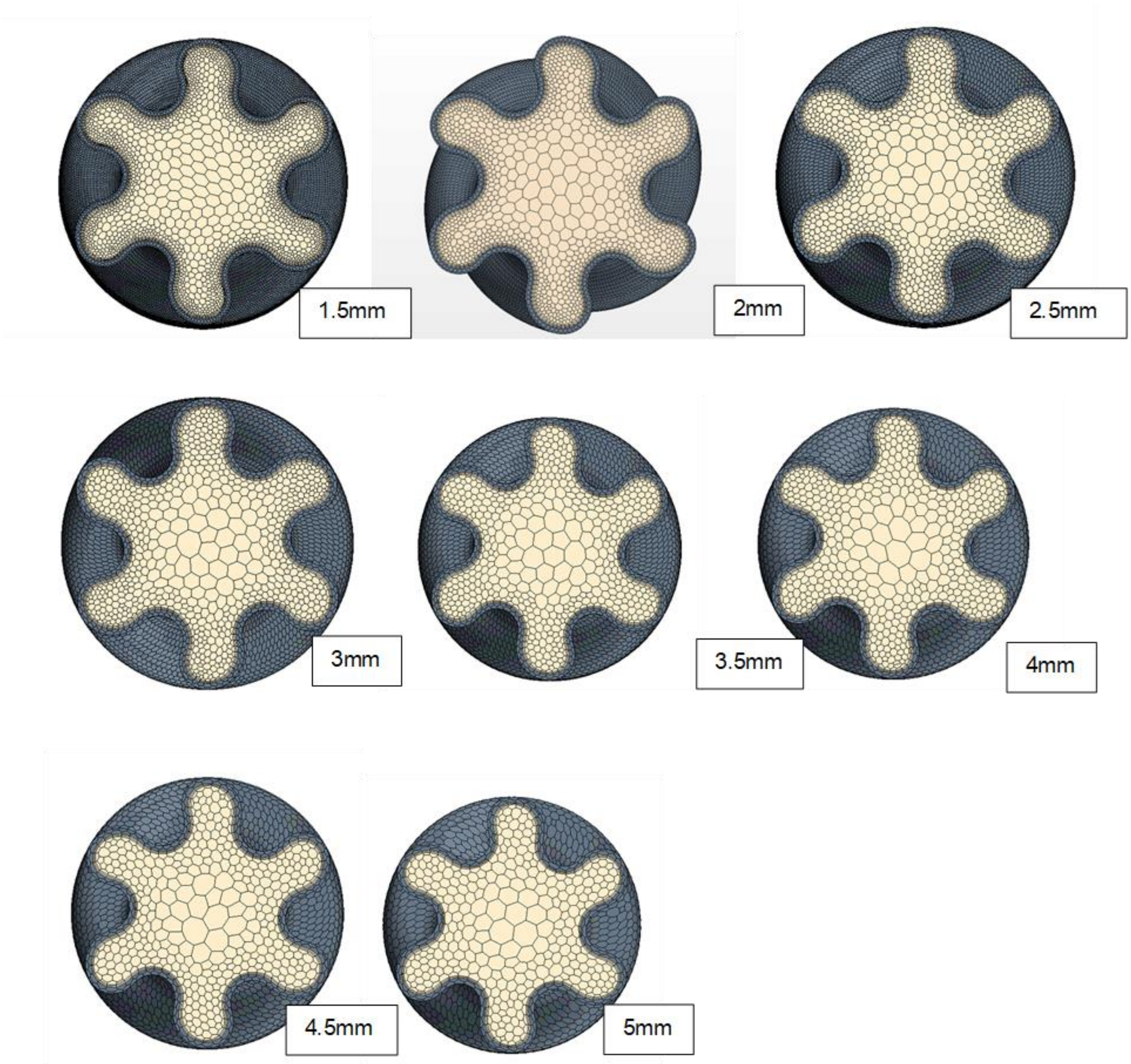

Figure 3-24: GVI mesh selection

The parameters considered for analysis are the Nusselt number and the pressure drop of the simulation. The results obtained from the simulation with 1.5mm base size is used as a reference, since this is the finest mesh size that is computationally allowed for the study. The results of the GVI is listed in Table 3-5 below;

Table 3-5: GVI results

Grid verification Index			
Base Size [mm]	**Nusselt number**	**% difference from 1.5mm**	**Cells**
1,5	270,641	**0,00000%**	20 381 202
2	267,477	**1,16911%**	9 114 953
2,5	264,308	**2,34000%**	3 063 148
3	262,16	**3,13374%**	2 895 280
3,5	259,009	**4,29798%**	1 995 403
4	257,549	**4,83759%**	1 495 809
4,5	250,638	**7,39101%**	1 168 686
5	249,052	**7,97706%**	875 344

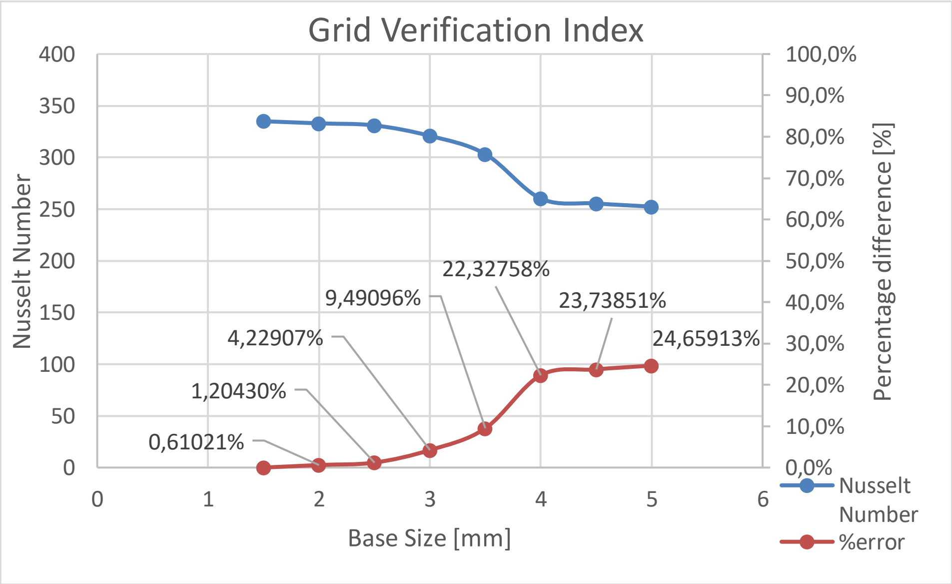

Figure 3-25: GVI of Base Size value

As illustrated in Figure 3-25 above, it is notable that with an increase in cells, the Nusselt number decreases and the difference between the simulations begin to minimise. It is worth mentioning that with the cell increase, the computation time also increases. From the base size value of 2.5mm and smaller, the value of the Nusselt number is almost constant, therefore, the base size value of 2mm is selected to insure consistency in the Nusselt number.

3.4 Calibration

In the aforementioned sections, the physics and mesh selected for the simulation of the HCFT-HX are determined and verified. Ensuing Figure 3-26 presents an overview of the physics and mesh selection. This study explores the effect of flute pitch and depth on the fluid's thermal properties. To ensure that any enhancement of the HCFT-HX is captured and that the simulation model truly reflects the realistic HCFT-HX, the simulation requires calibration. The calibration of the simulation model is conducted with experimental data obtained on the HCFT-HX. The data is captured in a study that investigated the possibility of simulating the flow of a HCFT-HX with analytical procedures [65].

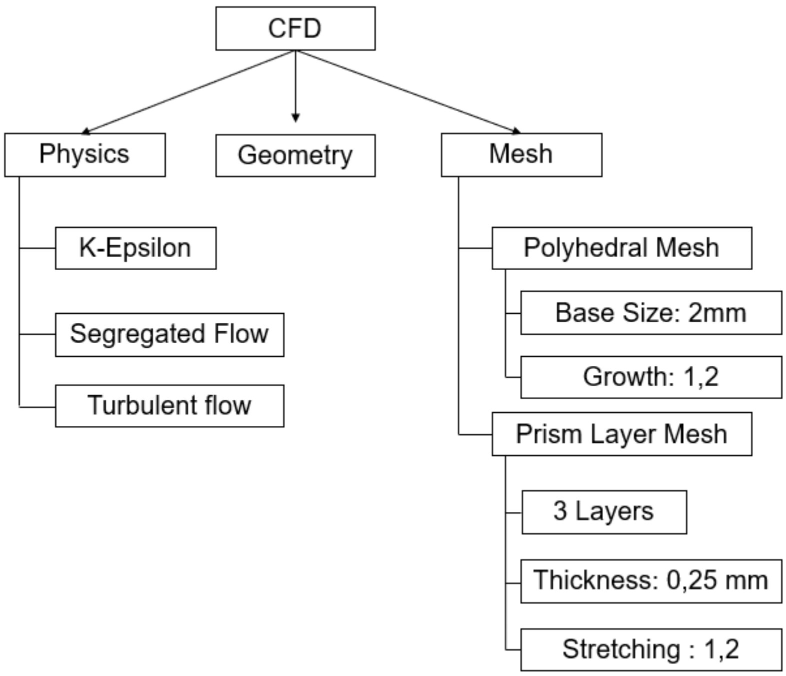

Figure 3-26: Model development

To ensure that the contact area of the fluid and the pipe is adequate, the temperature is used to calibrate the model. The experimental data obtained is the inlet and outlet temperature as well as the mass flow and are captured with the following equipment;

- Mass flow: Endress and Hauser Promag 50 transmitter with Promag P sensor [65]
- Temperature: Three-wire PT 100 temperature sensor [65]

In order to simulate the HCFT-HX, the thermal energy transferred into the fluid needs to be calculated. With the temperature and mass flow known, the thermal energy (heat) transferred to the water may be calculated with equation [3-13] by considering the specific heat (cp) as $4.182\ [kJ/kg.K]$. Five data sets are taken and illustrated in Table 3-6 below.

Table 3-6:Experimental data captured by Vermooten et al. [65]

Test	*Heat [kW]*	*Temperature in [C]*	*Temperature out [C]*	*Mass flow [kg/s]*
1	40,02925896	15,73801653	45,76528926	0,31877
2	33,67482574	15,542148	31,776033	0,49601
3	33,6005842	15,17024973	40,88264463	0,31248
4	33,454281	15,0424876	49,0727272	0,23507
5	39,37263	15,5231405	30,44876033	0,63078

With the mass flow captured in the experimental tests, the boundary selection is constructed as follows;

- Mass flow inlet
- Pressure outlet

The constructed mesh of the simulated HCFT-HX model is explicitly stipulated in Chapter 3.3.2, comprising a base size of 2mm, prism layer thickness of 0.25mm and a prism layer of 3. The model is illustrated in Figure 3-27 below.

Figure 3-27:Simulation model of HCFT-HX

The outlet temperature of the simulated model is listed in ensuing Table 3-7. The percentage error listed in Table 3-7 is calculated by equation [3-25] described below;

$$\%\boldsymbol{error} = \frac{\boldsymbol{Experimental - Simulated}}{\boldsymbol{Experimental}} \quad \textbf{[3-25]}$$

Table 3-7: Entire of HCFT-HX CFD simulation data.

	Test	Outlet Temperature [C]	Percentage Error
Entire heat exchanger	**1**	45,38	0,8562%
	2	31,77	0,00797%
	3	40,88	0,00207%
	4	49,08	0,00545%
	5	30,45	0,00020%

In this study, the effects of pitch and depth flute on the internal fluid's thermal properties are investigated. As a result, the temperature of the simulation model is near perfect with a maximum %error of 0.85%. Therefore, the simulated model may be deemed to be calibrated appropriately and that any enhancements made on the geometry are reflect in the simulated results.

As stated in the limitation of the study in Chapter 1, computational capacity is limited, and the enhancements of the heat exchanger may be time-consuming if the heat exchanger is simulated in its entirety. Thus, a single revolution of the heat exchanger is used to illustrate the effects of the parameters on the thermal performance of the heat exchanger. In Figure 3-28, the entire heat exchanger and a single revolution are illustrated.

Figure 3-28: Entire HCFT-HX with 4.5 coil revolutions (left) and a single revolution (right)

To verify that the sectional heat exchanger represents the entire heat exchanger, the sectional heat exchanger is also calibrated with the same experimental data. The data in Table 3-8 is divided by 4,5 as the entire heat exchanger consists of 4,5 revolutions. The data used to calibrate the sectional heat exchanger is illustrated in Table 3-8 below.

Table 3-8: Sectional experimental data.

Test	*Heat Flux [W]*	*Temperature in [C]*	*Temperature out [C]*	*Mass flow [kg/s]*
1	8895.39	15.74	22.41	0,31877
2	7483.29	15.54	19.15	0,49601
3	7466.80	15.17	20.88	0,31248
4	7434.28	15.04	22.60	0,23507
5	8746.47	15.52	18.84	0,63078

It is important to note that the same mesh and physics are applied to the sectional model of the HCFT-HX. The simulated data is given in Table 3-9 below;

Table 3-9: Sectional simulated data.

	Test	**Outlet Temperature [C]**	**Percentage Error**
Section of heat exchanger	**1**	22,41	0,005550%
	2	19,13	0,104326%
	3	20,88	0,035507%
	4	22,60	0,039651%
	5	18,79	0,277840%

Considering preceding Table 3-9, it may be noted that the simulated temperature is ~~also~~ less than 1% of the experimental data, indicating that the model may well represent the implemented alterations accurately.

3.5 Concluding remarks

This chapter aims to illustrate the procedure of developing the simulation model that will be used to simulate the alterations on the current HCFT-HX. The physics model is verified with a smooth tube simulation in EES and CFD. The percentage error between the CFD and EES was less than 3% from the EES results, which represented the analytical approach.

The cross-sectional geometry as well as the flute pitch are verified with a polymer 3D printed version of the CAD. The printed model is compared to a cut-out section of the HCFT-HX and alterations are made until the geometry is identical. The mesh of the simulations is verified with a GVI, the cell count of the simulation is deemed efficient with 9 million cells in a single revolution of the HCFT-HX.

The simulation model is then validated with experimental data obtained captured in a study conducted by Vermooten *et al*. [65]. The simulation and experimental data varied with less than 1% for the entire heat exchanger as well as a single revolution. The following chapter will comprise the alterations made to the parameters of the HCFT-HX.

CHAPTER 4: RESULTS

Chapter 4 discusses the results from this study when enhancing the HCFT-HX by altering the flute depth and flute pitch.

4.1 Impact of parameters on thermal performance

The previous chapters elaborate on the methods employed to calibrate and verify the CFD model. This chapter discusses the effect of the flute depth and pitch on the thermal properties of the HCFT-HX. The main thermal parameter that is utilised to determine the effects of the flute depth and pitch is the dimensionless Nusselt number. In numerous literature sources, the Nusselt number is also used to determine the effect of the heat transfer enhancements as it provides a dimensionless value of the heat transfer capabilities of a heat exchanger [15], [16], [66].

The purpose of this study is to determine the effect of flute depth and pitch on a HCFT-HX inner fluid's thermal performance. The literature review concludes that flute pitch and depth have the greatest impact on the thermal properties of the internal fluid. In Figure 4-1 the original parameters of the fluted tube are identified;

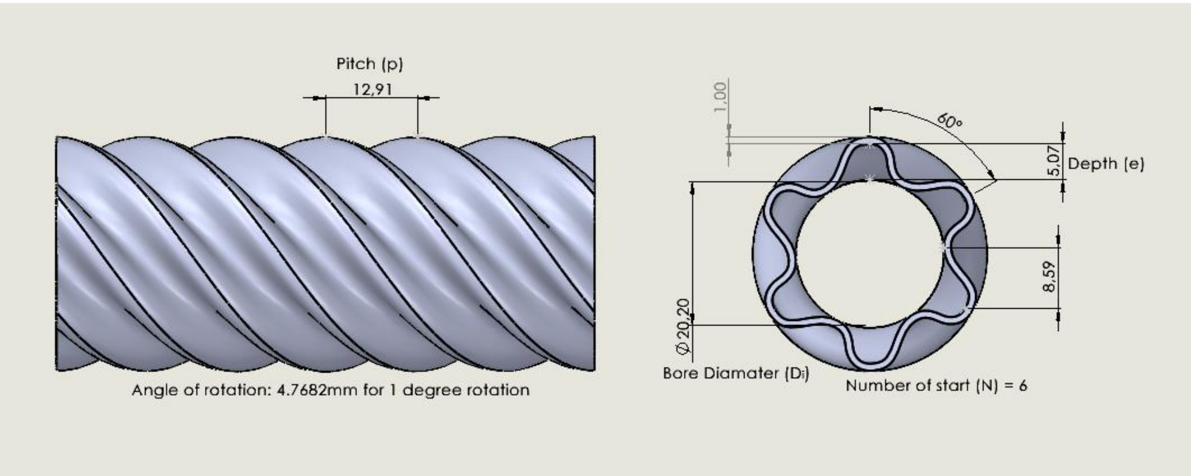

Figure 4-1: Original dimensions of the fluted tube evaluated

Sixteen HCFT-HX sections are created in CAD with altering flute pitch and depth. The pitch and depth values are selected based on the literature review where several indicate that in a straight fluted tube an increase in flute depth will result in an increase in heat transfer [19], [30], [67]. Figure 4-2 illustrates the cross-sections of the enhanced tubes, while Table 4-1 presents the flute depth and pitch that this study considers for investigation.

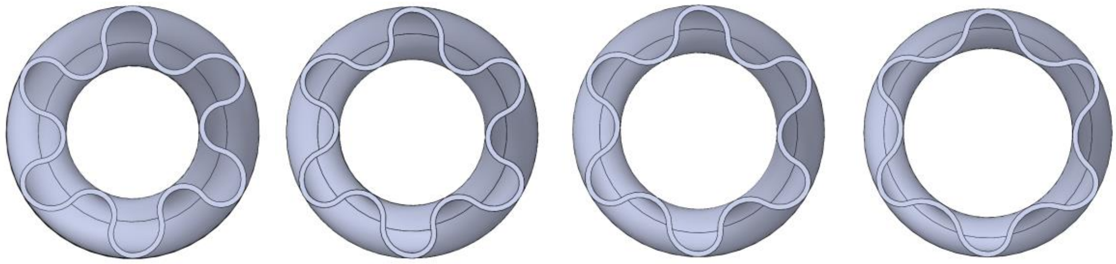

Depth: 7.17mm — Name: D7 | Depth: 6.28mm — Name: D6 | Depth: 5.58mm — Name: D5 | Depth: 4.59mm — Name: D4

Figure 4-2: Cross-sections of enhanced tubes

As illustrated in Figure 4-2, the depth is increased from right to left with a depth of 4.59mm, representing the shallowest depth and the largest depth of 7.17mm. The original HCFT-HX's depth is located between sections D5 and D4. Therefore, the study comprises sixteen different configurations each containing a different depth and pitch combination.

Table 4-1: Parameters of enhanced tubes

	Depth			
	7.17 [mm]	6.28[mm]	5.58 [mm]	4.59 [mm]
Pitch	9[mm]	9[mm]	9[mm]	9[mm]
	10[mm]	10[mm]	10[mm]	10[mm]
	11[mm]	11[mm]	11[mm]	11[mm]
	12[mm]	12[mm]	12[mm]	12[mm]

The study analyses the thermal properties, namely; Nusselt number, velocity and turbulent kinetic energy of the internal fluid and how the parameters listed in Table 4-1 affect these properties. The results from these simulations will enable the choice of the optimal possible configuration of the parameters to enhance the heat transfer of the heat exchanger. The following input values illustrated in Table 4-2 are used to simulate the enhanced pipes.

Table 4-2: Input values of CFD simulation.

Parameter	Value	Unit
Mass flow	0.5	Kg/s
Inlet Temperature	15	℃
Gauge pressure at inlet	0	Pa
Heat Source	8000	W

4.1.1 Nusselt number

The first thermal property analysed is the Nusselt number that provides a ratio of convective heat transfer over the conductive heat transfer [52], [53]. To better understand the quantitative value of the Nusselt number, a Nusselt number value of 1 represents pure conductive heat transfer, a large Nusselt number (being larger than 100) corresponds to active convective flow associated with turbulent flow [53].

As stated in Chapter 3, the Nusselt number is determined for each mesh cell, hence, to obtain an average of the Nusselt number, a "Surface Average" report on the interface between the solid and liquid regions are used to obtain the Nusselt number value for each enhancement. In Table 4-3 below, the values of the different pitch and depth of the fluted tubes are illustrated. Also, the Nusselt number versus flute pitch is demonstrated in ensuing Figure 4-3.

Table 4-3 Nusselt number of enhanced tubes

Depth [mm]	7D	6D	5D	4D
Pitch [mm]	$\boldsymbol{Hydraulic\ diameter}$: $\mathbf{0,0148}\ [\boldsymbol{m^2}]$	$\boldsymbol{Hydraulic\ diameter}$: $\mathbf{0,0117}[\boldsymbol{m^2}]$	$\boldsymbol{Hydraulic\ diameter}$: $\mathbf{0,0190}[\boldsymbol{m^2}]$	$\boldsymbol{Hydraulic\ diameter}$: $\mathbf{0,0191}\ [\boldsymbol{m^2}]$
9	449,57	408,21	405,85	364,49
10	435,12	383,00	348,16	345,20
11	398,25	376,65	330,75	315,46
12	364,77	314,78	303,17	284,35

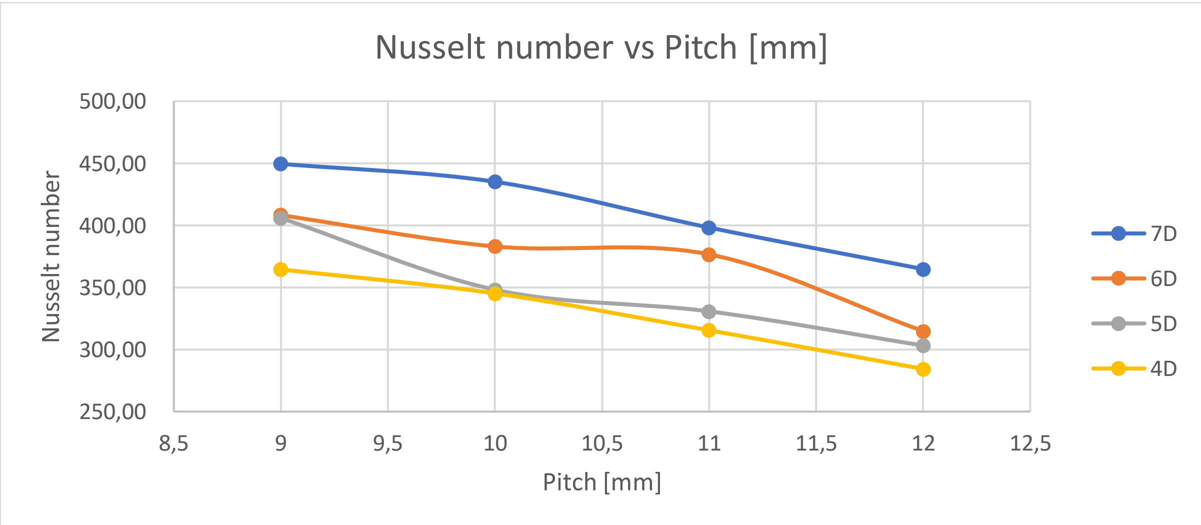

Figure 4-3: Nusselt number versus flute pitch

Figure 4-3 illustrates that when the pitch increases the Nusselt number decreases, similarly to what is identified in literature [19]. The decrease in Nusselt number as the pitch increases is attributed to the decrease in turbulent flow of the fluid as the pitch increases. The turbulence in the fluid is discussed in the following section.

In Figure 4-4 the, Nusselt number of enhancements 5D and 6D is presented, illustrating that the Nusselt number for both sections stay almost constant between pitch 10mm and 11mm. To further investigate this occurrence, the velocity and temperature distributions of these enhancements may be examined.

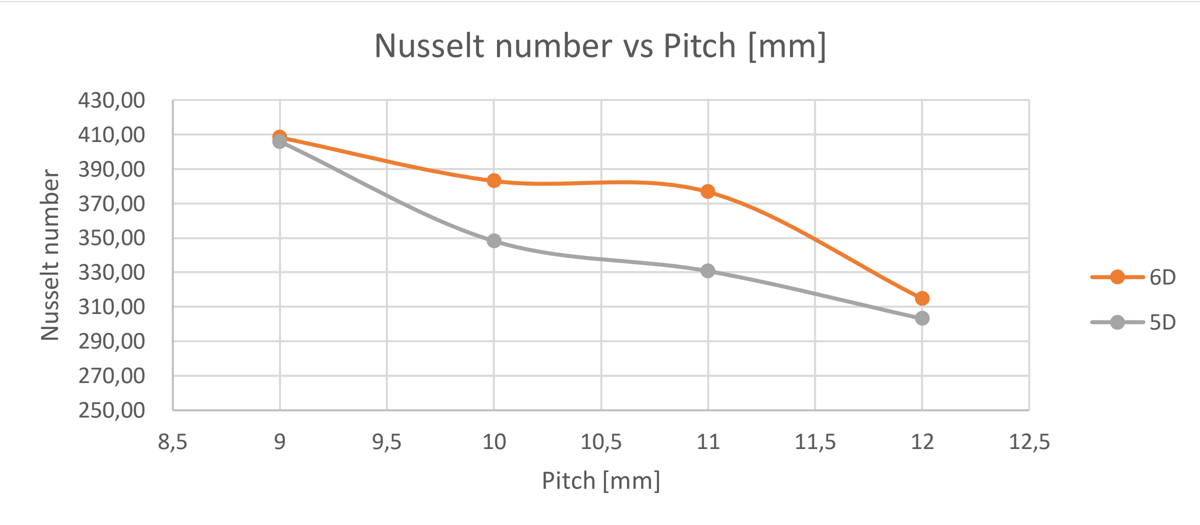

Figure 4-4: Difference in Nusselt number

Figure 4-5 represents the analysis of the temperature and velocity distribution at the outlet of the enhancements, indicating that the temperature and velocity profiles between pitch 10mm and 11mm are almost identical.

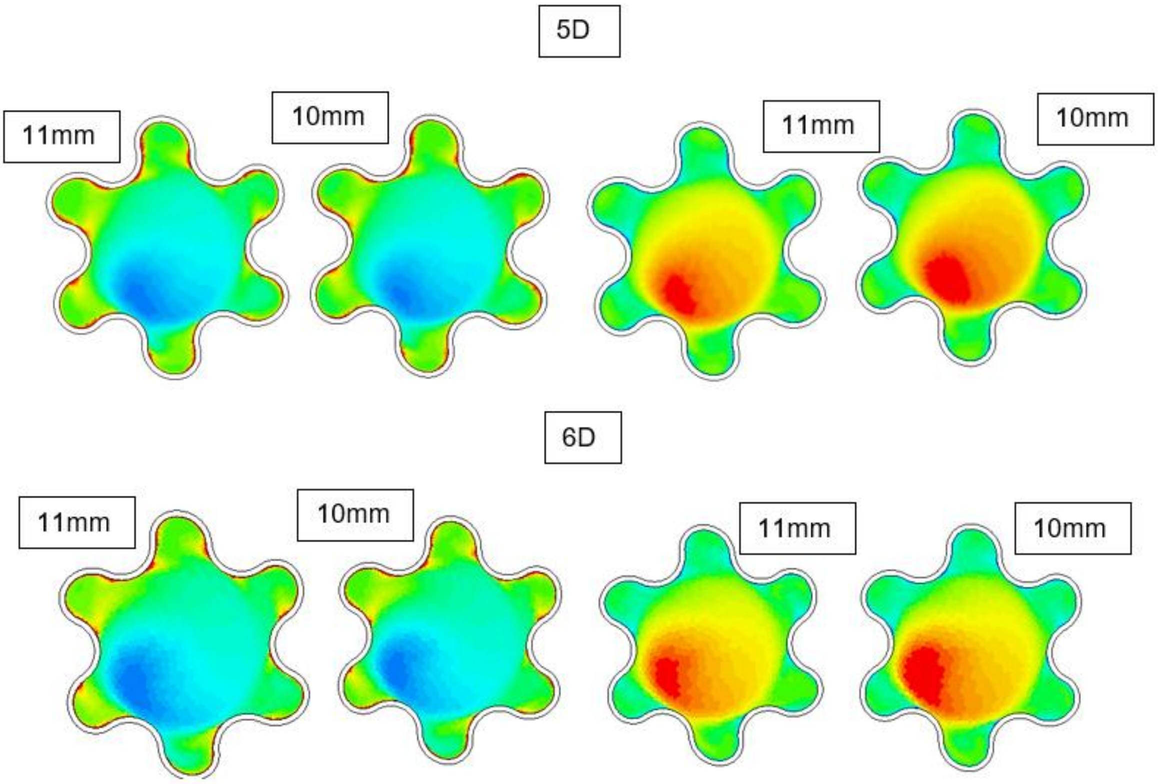

Figure 4-5: 6D (left) and 5D(right) temperature(left) and velocity(right) distribution.

The occurrence in enhancements 5D and 6D is a result of the combination of flute depth and flute pitch of 10mm and 11mm that provide similar flow patterners. In illustrating the fluid's flow patterns, the vorticity of the fluid may be examined. Vorticity is defined as the "whirling motion of a fluid", where an increase in vorticity is considered to represent a heat transfer enhancement [68]. Mathematically, the vorticity of a velocity field is described by equation [4-1] as the curl of a velocity fields;

$$\bar{\omega} = \bar{\nabla} \times \bar{u} \qquad [4\text{-}1]$$

The vorticity of the 4 enhancements at 11mm pitch are illustrated in Figure 4-6 below, with red representing a high vorticity, blue a low vorticity and white vorticity below 50 [rotations/s].

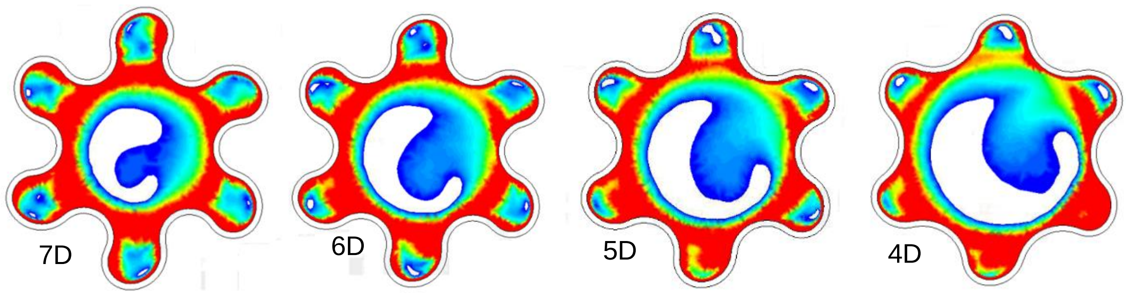

Figure 4-6: Vorticity in the different pipes at 11mm pitch.

It is notable that the flow pattern in 6D and 5D is similar with an 11mm pitch. As a result, the study argues that a HCFT-HX the thermal enhancement is lost in 5D and 6D when comprising a pitch between 10mm and 11mm. The decrease in Nusselt number as the pitch increases is attributed to the decrease in turbulent flow of the fluid. This may be described through the turbulent kinetic energy that is extensively analysed in the following section.

4.1.2 Turbulent Kinetic Energy

In turbulent flow, the intensity of the turbulence present is directly related to the turbulent kinetic energy [69]. Turbulent kinetic energy is defined as the mean kinetic energy per unit mass associated with turbulent flow [45]. The turbulent kinetic energy of section 7D is illustrated in Figure 4-7.

The turbulent kinetic energy is captured at the outlet of the enhancement with a surface average report, and the vorticity of the fluid is sketched as arrows on top of the cross-section. This assists in the illustration of the fluid motion inside the section where a density of the arrows correlate to the intensity of vorticity.

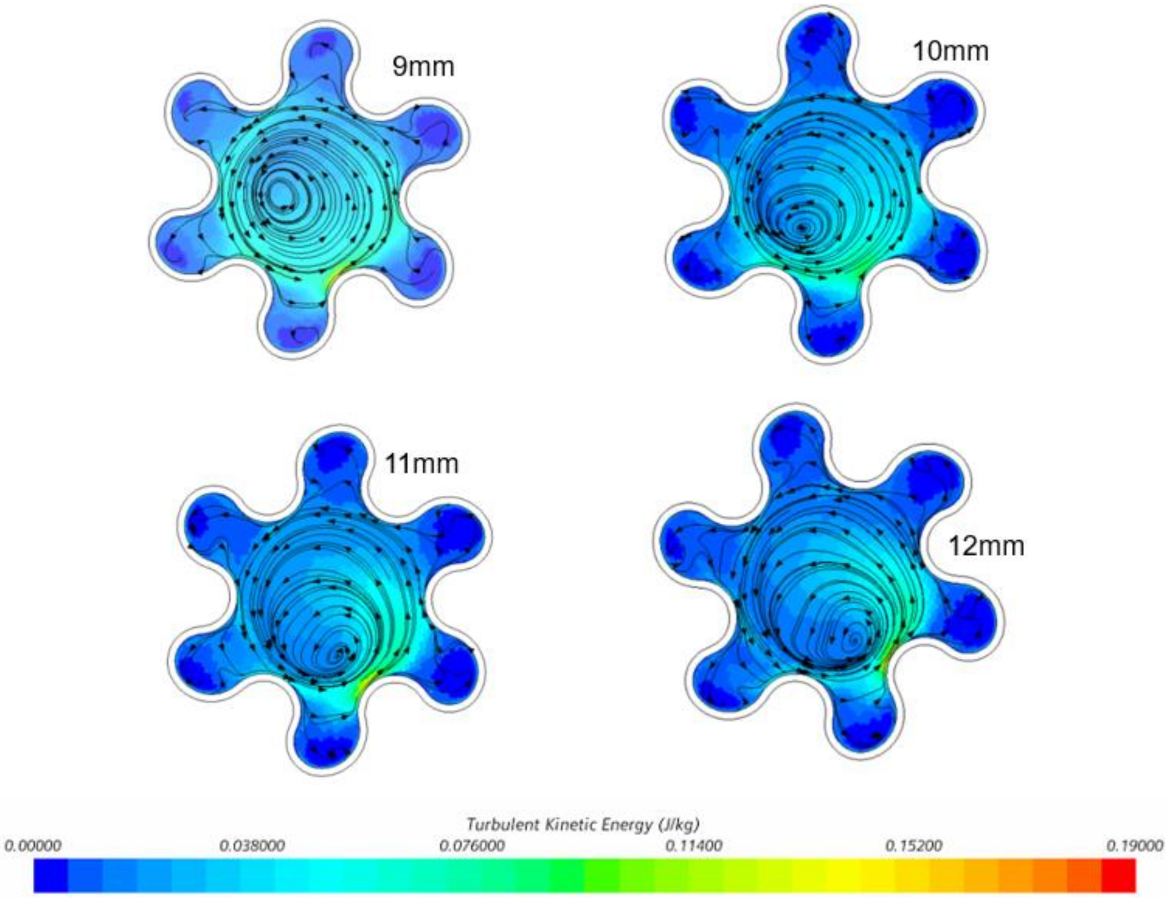

Figure 4-7: Turbulent Kinetic energy and Vorticity streamlines of pipe 7D.

In Figure 4-7 above, it can be seen that with an increase in pitch the overall turbulent kinetic energy decreases on the cross-section. A similar trend appears in all the sections with regards to turbulent kinetic energy. The surface average of the turbulent kinetic energy on the outlet region is illustrated in Figure 4-8 and Table 4-4 below;

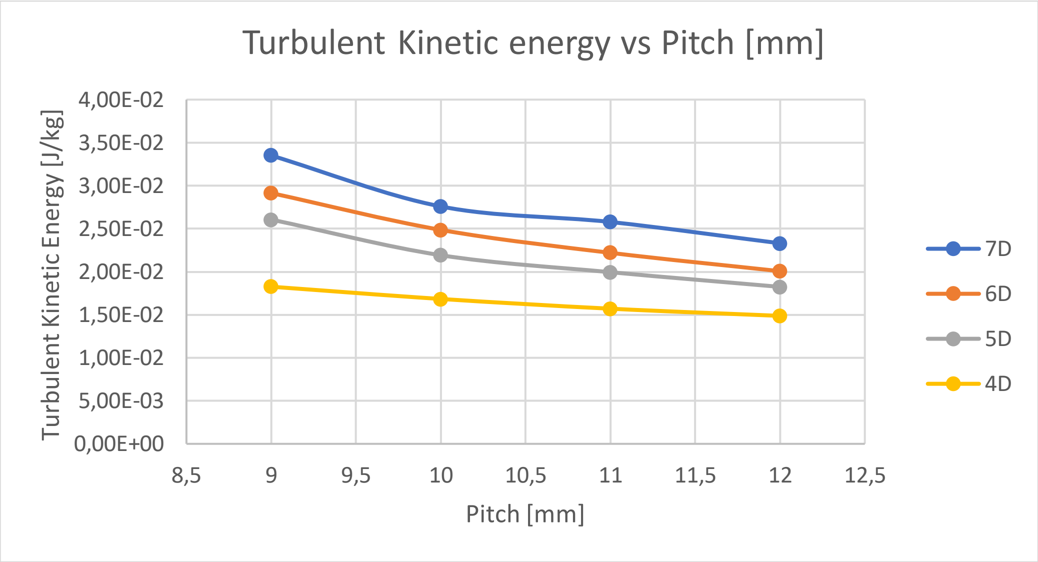

Figure 4-8: Turbulent Kinetic energy on the outlet of the pipes

Table 4-4: Turbulent kinetic energy

Depth [mm]	**7D**	**6D**	**5D**	**4D**
Pitch [mm]	$[\frac{J}{kg}]$	$[\frac{J}{kg}]$	$[\frac{J}{kg}]$	$[\frac{J}{kg}]$
9	$3{,}35 \times 10^{-2}$	$2{,}91 \times 10^{-2}$	$2{,}61 \times 10^{-2}$	$1{,}83 \times 10^{-2}$
10	$2{,}76 \times 10^{-2}$	$2{,}49 \times 10^{-2}$	$2{,}19 \times 10^{-2}$	$1{,}68 \times 10^{-2}$
11	$2{,}58 \times 10^{-2}$	$2{,}22 \times 10^{-2}$	$1{,}99 \times 10^{-2}$	$1{,}57 \times 10^{-2}$
12	$2{,}33 \times 10^{-2}$	$2{,}01 \times 10^{-2}$	$1{,}82 \times 10^{-2}$	$1{,}49 \times 10^{-2}$

Results of enhancement 7D with 9mm pitch identify that the turbulent kinetic energy is double on the outlet when compared to enhancement 4D that comprises a pitch of 12mm. This correlates to the findings in the Nusselt number discussion, where enhancement 7D with a 9mm pitch has the highest Nusselt number, while enhancement 4D with 12mm pitch has the lowest. Supporting the statement that when the flute depth decreases the flow becomes less turbulent, the study argues that a similar notion may be presented for the increase in pitch. Therefore, it may be concluded that altering the flute depth pitch results in an increase in turbulent flow.

4.1.3 Pressure Drop

Even though the effect of pressure drop is not be extensively researched in this study, it is worth noting that pressure drop has an effect on the overall efficiency of a heat exchanger. The simulation of pressure drop is validated with the smooth tube comparison between EES and CFD in Chapter 3.1.3. Therefore, the pressure drop simulated in the enhancements may be conceived as an accurate estimation of the pressure drop that may be present under actual operating conditions. The Figure 4-9 below illustrates the pressure distribution (in colour) on the outlet of enhancement 7D that has the highest Nusselt number of the sections. Along with the pressure drop, the vorticity vector is sketched on top of the cross-section as arrows to illustrate the flow direction of the fluid.

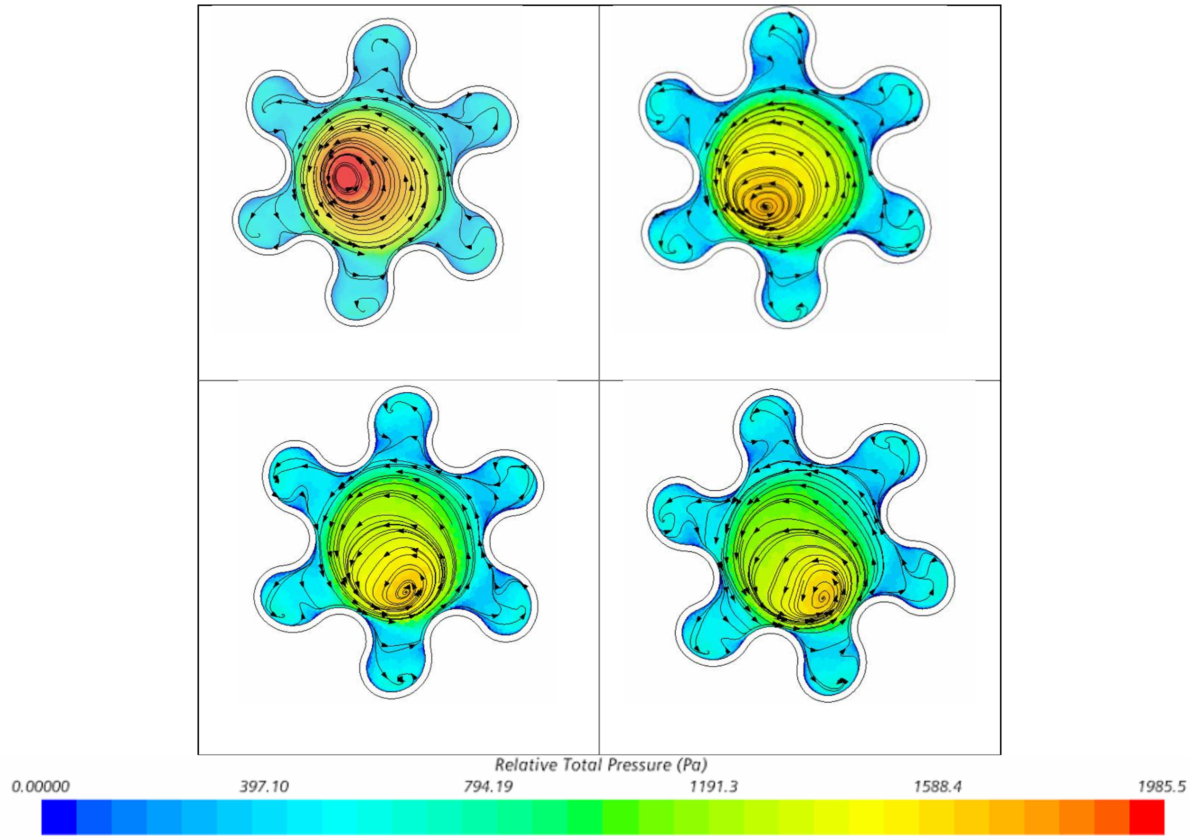

Figure 4-9:Pressure distribution

Figure 4-9 identifies that the higher-pressure regions are identical with the higher vorticity regions in the fluid. The pressure drop across the sections is determined through a surface average on the outlet and illustrated in Table 4-5;

Table 4-5: Pressure drop over the pipes.

Depth [mm]	7D	6D	5D	4D
Pitch [mm]	**Pressure drop [Pa]**	**Pressure drop [Pa]**	**Pressure drop [Pa]**	**Pressure drop [Pa]**
9	7 957,07	5 909,12	4 761,44	3 134,46
10	6 168,24	4 672,73	3 743,19	2 795,81
11	5 557,47	4 149,84	3 329,40	2 521,23
12	4 995,55	3 783,34	3 009,85	2 290,75

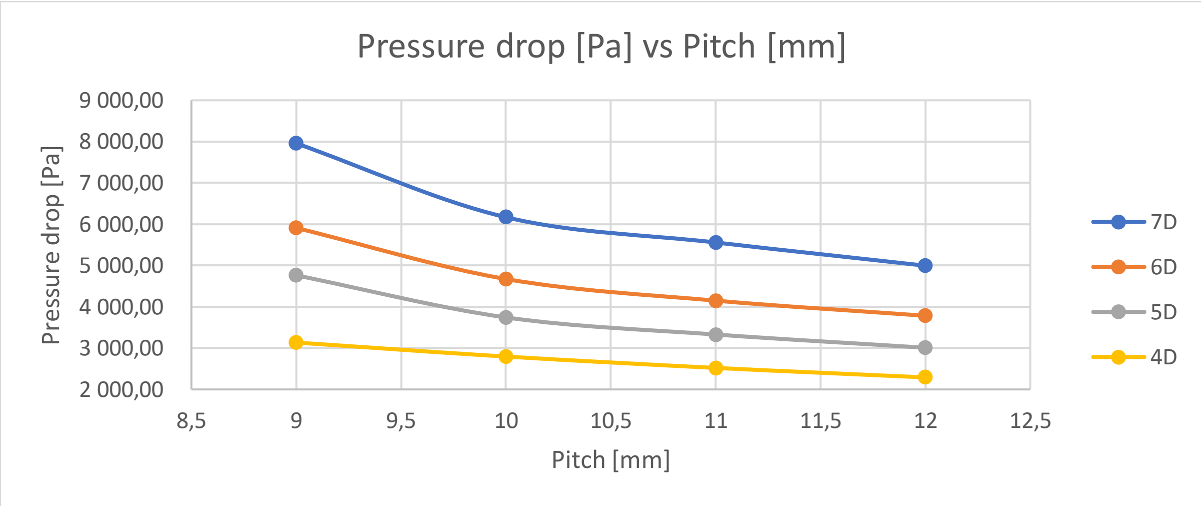

Figure 4-10: Graph of pressure drop over enhanced pipes

A clear decline in pressure drop is notable as the pitch increases and the depth decreases, similarly than the investigated literature [19], [20], [26].

4.1.4 Concluding remarks on parameters

As stated in the previous sections, the enhancements with the highest and lowest thermal performance is enhancement 7D with pitch 9mm and enhancement 4D with a 12mm pitch, respectively. To further illustrate the effect that the parameters have on the internal fluid, the velocity in these sections are plotted at the same velocity scale in Figure 4-13 below.

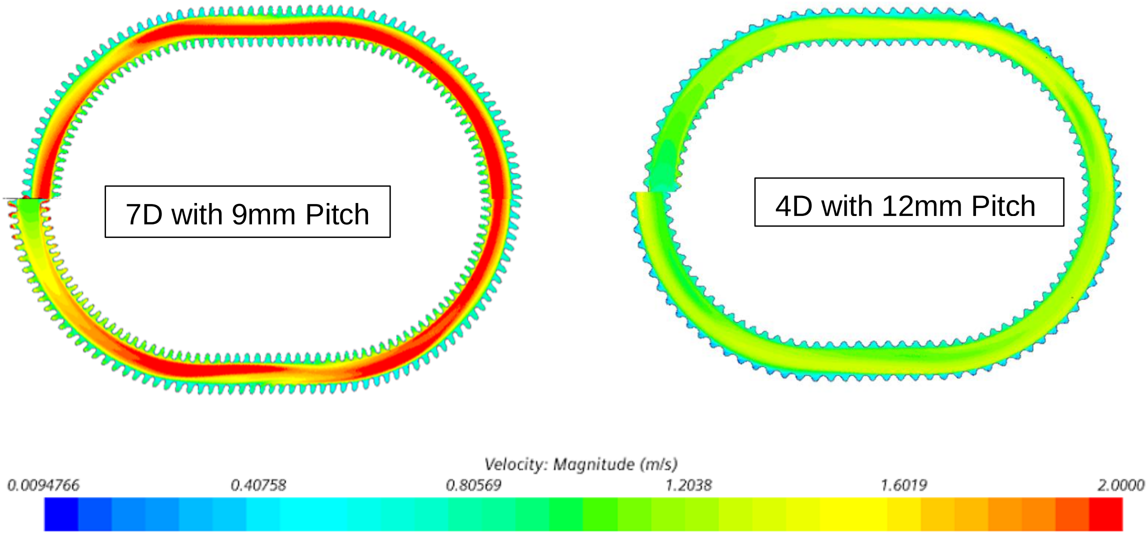

Figure 4-11: Velocity distribution of pipes 7D with 9mm pitch and 4D with 12mm pitch

As proposed, the bulk flow of enhancement 7D comprises a higher velocity than enhancement 4D and this may be contributed to the enhanced thermal performance of 7D over 4D. Table 4-5 identifies that enhancement 7D with a 9mm pitch has the highest pressure drop, while enhancement 4D with a 12mm pitch has the lowest pressure drop. The pressure drop of 7D has a 247% increase when compared to 4D. Finally, 7D comprising a 9mm pitch indicates that the thermal performance is enhanced by 58% when compared to 4D with a 12mm pitch.

In summarising the above findings, a rating matrix (Table 4-6) is constructed to present the effect of the parameters on the Nusselt number and pressure drop are illustrated;

Table 4-6: Rating Matrix

Nusselt number

Pressure drop

Pitch: 12mm Depth: 4,59mm	Pitch: 12mm Depth: 5,58mm	Pitch: 12mm Depth: 6,28mm	Pitch: 12mm Depth: 7,17mm
Pitch: 11mm Depth: 4,59mm	Pitch: 11mm Depth: 5,58mm	Pitch: 11mm Depth: 6,28mm	Pitch: 12mm Depth: 7,17mm
Pitch: 10mm Depth: 4,59mm	Pitch: 10mm Depth: 5,58mm	Pitch: 10mm Depth: 6,28mm	Pitch: 10mm Depth: 7,17mm
Pitch: 9mm Depth: 4,59mm	Pitch: 9mm Depth: 5,58mm	Pitch: 9mm Depth: 6,28mm	Pitch: 9mm Depth: 7,17mm

Nusselt number

Pressure drop

The table illustrates that by increasing the pitch, the pressure in addition to the Nusselt number decreases. Through increasing the depth, the pressure and Nusselt number increases accordingly.

4.2 Impact of AM

4.2.1 AM material

The effect of manufacturing the enhancements through AM and utilising Ti64 are discussed in the following chapter. As stated in Chapter 3, the efficiency of thermal energy moving though a solid is directly proportional to the thermal conductivity of the solid. The study conducted by Jordaan et al. [70] determine the thermal conductivity of Ti64 manufactured through SLM.

In obtaining the thermal conductivity of the samples, the hot plate method is used, which consists of a Ti64 plate embedded between a temperature difference. The temperature difference is resultant from two copper plates operating at two different temperatures and monitored through a thermostat.

The study concludes that through implementing equation [3-7] and its subsequent simulation, the experimental value of 6.74W/m.K has a percentage deviation of 2.5% from simulated results. In supporting the latter, the manufacturers of the Ti64 powder also demonstrates that the material comprises a 6.6 W/m.K to 6.8 W/m.K thermal conductivity [71].

This study evaluates the effect of modifying the thermal conductivity to 6.74W/m.K on the thermal performance of the internal fluid. This is analysed through evaluating the effect it has on the temperature distribution in the internal fluid. Figure 4-12 below, demonstrates the effect of altering the thermal conductivity from a commercially pure titanium to Ti64, by illustrating the temperature on the outlet and interface of the fluid.

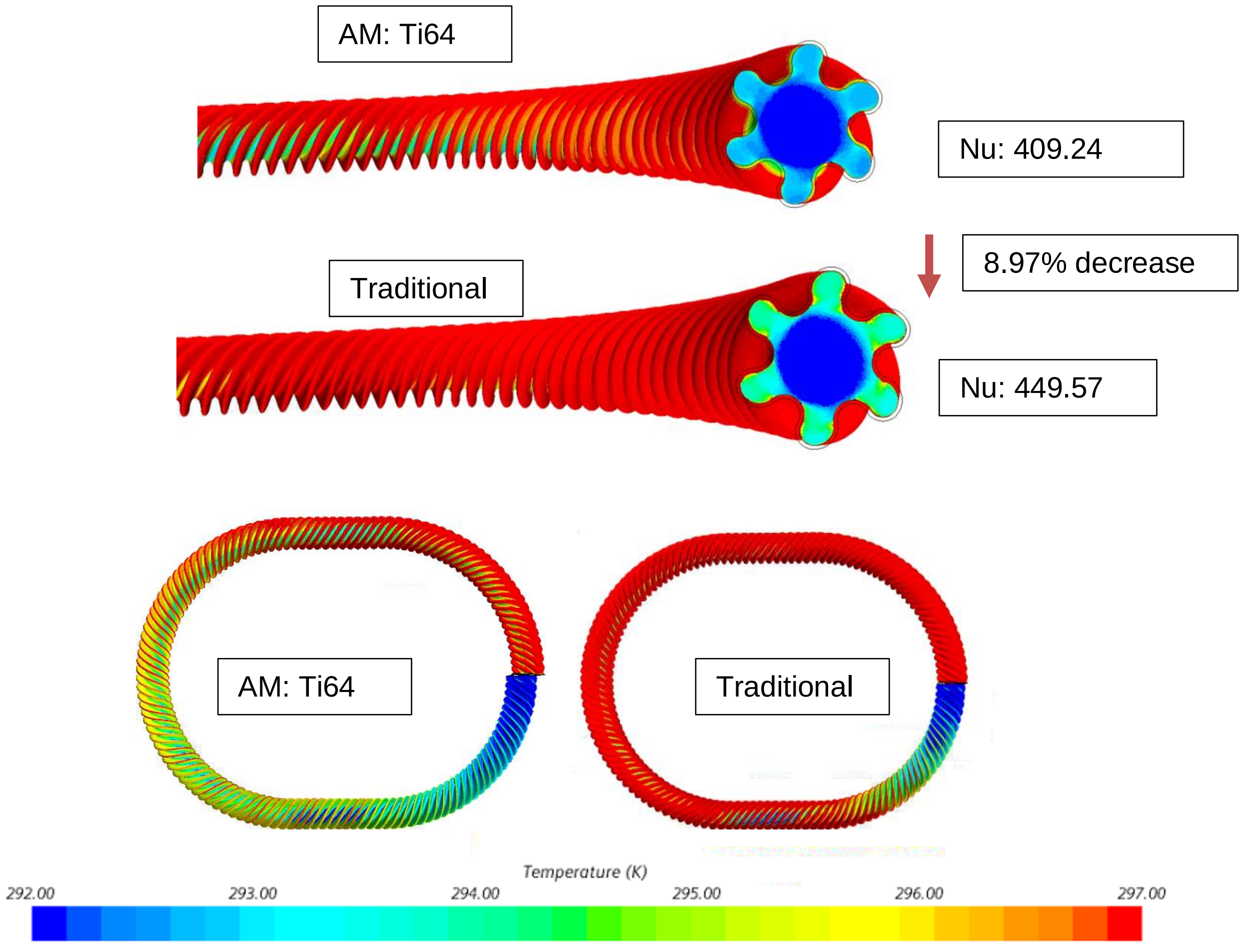

Figure 4-12:Effect on temperature distribution of AM Ti64 manufacturing compared to pure titanium

Evaluating the Nusselt number, a decrease of 8.972% is observed in the AM version. The effect of thermal conductivity on the temperature distribution of the fluid is also noticeable as the fluid has a lower overall temperature in the AM version. Alongside this, the fluid in the commercially pure titanium pipe reaches a higher temperature at an early stage, whereas the AM version only reaches the same peak temperature at the end of the section.

CHAPTER 5: CONCLUSIONS

Industry is continuously striving for more efficient heat exchangers. With the titanium HCFT-HX considered as an innovative solution, increasing its performance by utilising AM may well be beneficial to multiple industries. Currently limited research exists on titanium HCFT-HX's focusing on the effect that fluted geometry has on the inner fluid's thermal performance.
In the literature review it is determined that the flute depth and pitch have the greatest effect on the thermal performance of a fluted tube. As stated in the literature review, the use of AM in heat exchangers have proven to contribute promising results in thermally enhancing the heat exchangers.

The heat exchanger is constructed using CAD and simulated in STAR-CCM+ with a K-Epsilon physics model and "All y+" wall treatment. The mesh is verified with a grid verification index and a fluctuation of less than 1% is observed with a mesh base size of 2mm and a prism layer thickness of 0.25mm. The simulation model of the heat exchanger is subsequently calibrated with experimental data captured in the study of Vermooten *et al*. [65]. The calibration data of the simulation presents a %error of less than 1% from the experimental data and the model is therefore deemed calibrated.

The enhancement parameters are selected to comprise a pitch of 9mm, 10mm, 11mm, 12mm and a depth of 7.18mm, 6.28mm, 5.58mm and 4.58mm. The enhancements comprise a total of sixteen configurations and are simulated with uniform inputs; specifically mass flow of $0.5[kg/s]$, inlet temperature of $15°\mathrm{C}$ and a heat flux of $8000W$ on the outer surface of the sections. The Nusselt number is selected to be the fluid characteristic in which the thermal performance is measured, coupled with the turbulent kinetic energy, vorticity and temperature. The enhancement with the highest thermal performance (58% higher than the lowest performer) is the fluted tube with a depth of 11mm and a pitch of 9mm. This is a result of the increase in turbulent energy in the fluid, accompanied by the increase in thermal performance where the highest pressure drop is observed in the same fluted tube (pitch of 9mm and depth of 7.18mm) with an increase of 247% higher than that of the lowest performer. In conclusion, the study indicates that flute depth and pitch have a significant effect on the thermal performance of the internal fluid of HCFT-HX. As the flute pitch is enlarged, the thermal performance decreases and pressure drop decreases. In contrast, by enlarging the flute depth the thermal performance is increased and the pressure drop increases.

The effect of manufacturing the HCFT-HX through AM and utilising Ti64~~,~~ results in an 8.972% decrease in Nusselt number. This is due to the decrease in thermal conductivity from commercially pure titanium to its alloy counterpart. The study identifies that Ti64 is not a thermal enhancement over commercially pure titanium, however, the cost and availability of Ti64 may be more attractive. The study therefore concludes that utilising Ti64 though AM is not beneficial in thermally enhancing a titanium HCFT-HX.

5.1 Recommendations

In response to the preceding conclusions, the study recommends the following for future studies;

- This study demonstrates that flute pitch and depth play a significant role in enhancing the thermal performance of HCFT-HX, however, the tube 7D with 9mm pitch should be manufactured through AM and experimentally tested.
- The effect on thermal performance of enlarge surface roughness in AM parts should be investigated.
- Design for AM should be employed in the enhancement of the HCFT-HX.

CHAPTER 6: REFERENCES

[1] D. Jafari and W. W. Wits, "The utilization of selective laser melting technology on heat transfer devices for thermal energy conversion applications : A review," *Renew. Sustain. Energy Rev.*, vol. 91, no. March, p. 420;, 2018.

[2] M. Wong, S. Tsopanos, C. J. Sutcliffe, and I. Owen, "Selective laser melting of heat transfer devices.," *Rapid Prototyp. J.*, vol. 13, no. 5, p. 291, 2007.

[3] R. N. Christensen and S. Garimella, "Spirally-fluted tubes and enhanced tubes in confined crossflow. Part II: Fluted tube annuli," Ohio State, 1990.

[4] A. Gagneja and S. Pundhir, "Heat Pumps and Its Applications," *Int. J. Adv. Chem. Eng. Biol. Sci.*, vol. 3, no. 1, pp. 2–5, 2016.

[5] P. G. Rousseau, M. Van Eldik, and G. P. Greyvenstein, "Detailed simulation of fluted tube water heating condensers.," vol. 26, pp. 232–239, 2003.

[6] C. Young, "The use of titanium for heat transfer in the chemical processing industry," 2020. [Online]. Available: https://www.heat-exchanger-world.com/mobile/webarticles/2020/02/19/the-use-of-titanium-for-heat-transfer-in-the-chemical-processing-industry.html.

[7] M. Shunmugavel, A. Polishetty, M. Goldberg, R. Singh, and G. Littlefair, "A comparative study of mechanical properties and machinability of wrought and additive manufactured (selective laser melting) titanium alloy – Ti-6Al-4V," *Rapid Prototyp. J.*, vol. 23, no. 6, pp. 1051–1056, 2017.

[8] U. Scheithauer *et al.*, "Potentials and Challenges of Additive Manufacturing Technologies for Heat Exchanger," in *Advances in Heat exchangers*, L. C. Gómez and V. M. V. Flores, Eds. Germany: IntechOpen, 2018, pp. 42–61.

[9] R. Gregorig, J. Kern, and K. Turek, "Improved correlation of film condensation data based on a more rigorous application of similarity parameters," *Wärme- und Stoffübertragung*, vol. 7, no. 1, pp. 1–13, Mar. 1974.

[10] R. L. Webb, "A generalized procedure for the design and optimization of fluted gregorig condensing surfaces," *J. Heat Transfer*, vol. 101, no. 2, pp. 335–339, 1979.

[11] H. Llewellyn, “Design and Analysis of a 5-MW Vertical-Fluted-Tube Condenser for Geothermal Applications,” Oak Ridge, Tennessee, 1982.

[12] W. M. Rohsenow, J. R. Hartnett, and Y. I. Cho, *HANDBOOK OF HEAT TRANSFER*, 3rd ed. McGraw-Hill.

[13] S. S. Kruthiventi, N. G. Rasu, and Y. V. H. Rao, “Coiled Tube Heat Exchangers -,” *Int. J. Mech. Eng. Technol.*, vol. 9, no. 1, pp. 895-904;896.

[14] T. Mat Lazim, Z. S. Kareem, M. N. M. Mohd Jaafar, S. Abdullah, and A. F. Abdulwahid, “Heat transfer enhancement in spirally corrugated tube,” *Int. Rev. Model. Simulations*, vol. 7, no. 6, pp. 970–978, 2014.

[15] T. M. L. M. N Nazri S. Abdulla, Z. S. Kaeem, A.F. Abdulwahd TS - CrossRef, Ed., “Corrugation profile effect on heat transfer enhancement of laminar flow region.,” in *International Academy of Engineers*, 2015.

[16] V. Kongkaitpaiboon, P. Promthaisong, V. Chuwattanakul, K. Wongcharee, and S. Eiamsa-ard, “Effects of spiral start number and depth ratio of corrugated tube on flow and heat transfer characteristics in turbulent flow region,” *J. Mech. Sci. Technol.*, vol. 33, no. 8, pp. 4005–4012, 2019.

[17] L. Ya-xia, W. Jian-hua, W. Hang, K. Li-ping, and T. Xiao-hang, “Fluid Flow and Heat Transfer Characteristics in Helical Tubes Cooperating with Spiral Corrugation,” *Energy Procedia*, vol. 17, pp. 791–800, 2012.

[18] K. Thulukkanam, *Heat Exchanger Design Handbook*. 2013.

[19] Z. jiang Jin, F. qiang Chen, Z. xin Gao, X. fei Gao, and J. yuan Qian, “Effects of pitch and corrugation depth on heat transfer characteristics in six-start spirally corrugated tube,” *Int. J. Heat Mass Transf.*, vol. 108, pp. 1011–1025, 2017.

[20] H. H. Balla, “Enhancement of heat transfer in six-start spirally corrugated tubes,” *Case Stud. Therm. Eng.*, vol. 9, no. January, pp. 79–89; 85, 2017.

[21] “Heat Transfer Analysis on Twisted Tube Heat Exchanger Technology,” vol. 5, no. 4, pp. 2642–2644, 2015.

[22] J. D. Bernardin, K. Ferguson, D. Sattler, and S. Kim, “The Design, Analysis, and

Fabrication of an Additively Manufactured Twisted Tube Heat Exchanger," in *Volume 2: Heat Transfer Equipment; Heat Transfer in Multiphase Systems; Heat Transfer Under Extreme Conditions; Nanoscale Transport Phenomena; Theory and Fundamental Research in Heat Transfer; Thermophysical Properties; Transport Phenomena in Materials Pr*, 2017, pp. 1–8.

[23] Y. Dong, L. Huixiong, and C. Tingkuan, "Pressure drop, heat transfer and performance of single-phase turbulent flow in spirally corrugated tubes," *Exp. Therm. Fluid Sci.*, vol. 24, no. 3–4, pp. 131–138, 2001.

[24] A. Barba, S. Rainieri, and M. Spiga, "Heat transfer enhancement in a corrugated tube," *Int. Commun. Heat Mass Transf.*, vol. 29, no. 3, p. 313, 2002.

[25] S. Pethkool, S. Eiamsa-ard, S. Kwankaomeng, and P. Promvonge, "Turbulent heat transfer enhancement in a heat exchanger using helically corrugated tube," *Int. Commun. Heat Mass Transf.*, vol. 38, no. 3, pp. 340–347, 2011.

[26] Z. S. Kareem, S. Abdullah, T. M. Lazim, M. N. Mohd Jaafar, and A. F. Abdul Wahid, "Heat transfer enhancement in three-start spirally corrugated tube: Experimental and numerical study," *Chem. Eng. Sci.*, vol. 134, pp. 746–757, 2015.

[27] Z. S. Kareem, M. N. Mohd Jaafar, T. M. Lazim, S. Abdullah, and A. F. Abdulwahid, "Heat transfer enhancement in two-start spirally corrugated tube," *Alexandria Eng. J.*, vol. 54, no. 3, pp. 415–422, 2015.

[28] v. d. Zimparov, N. L. Vulchanov, and L. B. Delov, "Heat transfer and friction characteristics of spirally corrugated tubes for power plant condensers—1. Experimental investigation and performance evaluation," *Int. J. Heat Mass Transf.*, vol. 34, no. 9, pp. 2187–2197, Sep. 1991.

[29] S. C. Lee, S. C. Nam, and T. G. Ban, "Performance of heat transfer and pressure drop in a spirally indented tube," *KSME Int. J.*, vol. 12, no. 5, pp. 917–925, Sep. 1998.

[30] L. Wang, D.-W. Sun, P. Liang, L. Zhuang, and Y. Tan, "Heat transfer characteristics of carbon steel spirally fluted tube for high pressure preheaters," *Energy Convers. Manag.*, vol. 41, no. 10, pp. 993–1005, Jul. 2000.

[31] U. M. Dilberoglu, B. Gharehpapagh, U. Yaman, and M. Dolen, "The role of additive manufacturing in the era of Industry 4 . 0," *Procedia Manuf.*, vol. 11, no. June, pp. 545–

554, 2017.

[32] J. O. Milewski, “Envision,” in *Additive Manufacturing of Metals*, 2017, pp. 1–6.

[33] K. V. Wong and A. Hernandez, “A Review of Additive Manufacturing,” *ISRN Mech. Eng.*, vol. 2012, pp. 1–10, 2012.

[34] A. Koptyug, L.-E. Rännar, M. Bäckström, M. S. S. Fager Franzén, and D. P. Dérand, “ADDITIVE MANUFACTURING TECHNOLOGY APPLICATIONS TARGETING PRACTICAL SURGERY,” *Int. J. Life Sci. Med. Res.*, vol. 3, no. 1, pp. 15–24, Feb. 2013.

[35] V. Bhavar, P. Kattire, V. Patil, S. Khot, K. Gujar, and R. Singh, “A review on powder bed fusion technology of metal additive manufacturing,” *Addit. Manuf. Handb. Prod. Dev. Def. Ind.*, no. September, pp. 251–261, 2017.

[36] S. M. Thompson, Z. S. Aspin, N. Shamsaei, A. Elwany, and L. Bian, “Additive manufacturing of heat exchangers: A case study on a multi-layered Ti–6Al–4V oscillating heat pipe,” *Addit. Manuf.*, vol. 8, pp. 163–174, 2015.

[37] W. Seiya and S. Zhang, “3D Printing as an Alternative Manufacturing Method for the Micro-gas Turbine Heat Exchanger,” pp. 1–71, 2015.

[38] D. J. Saltzman *et al.*, “Experimental comparison of a traditionally built versus additively manufactured aircraft heat exchanger,” *55th AIAA Aerospace Sciences Meeting*. American Institute of Aeronautics and Astronautics, Reston, Virginia, 22095BC.

[39] E, “Material Data Sheet: EOS Aluminium AlSi10Mg,” vol. 49, no. 0. EOS, pp. 1–5, 2014.

[40] K. S. Garde, “DESIGN AND MANUFACTURE OF AN OIL COOLER BY ADDITIVE MANUFACTURING,” UNIVERSITY OF MINNESOTA, 2017.

[41] D. Bacellar, V. Aute, Z. Huang, and R. Radermacher, “Design optimization and validation of high-performance heat exchangers using approximation assisted optimization and additive manufacturing,” *Sci. Technol. Built Environ.*, vol. 23, no. 6, pp. 896–911, 2017.

[42] “Extek: Products,” *Extek*. [Online]. Available: http://extek.com.cn/detail-2019722-14713-en.html. [Accessed: 05-Nov-2020].

[43] “A Guide to 3D Printing With Titanium - AMFG.” [Online]. Available:

https://amfg.ai/2019/06/18/titanium-3d-printing-guide/. [Accessed: 27-Jul-2020].

[44] "How Can Aerospace Benefit from 3D Printed Titanium Ti6Al4V," *Farinia Group*. [Online]. Available: https://www.farinia.com/additive-manufacturing/3d-materials/how-can-aerospace-benefit-from-3d-printed-titanium-Ti6Al4V. [Accessed: 16-Oct-2020].

[45] "Introduction to turbulence/Turbulence kinetic energy." [Online]. Available: https://www.cfd-online.com/Wiki/Introduction_to_turbulence/Turbulence_kinetic_energy.

[46] J. D. Jr.Anderson, *Computational Fluid Dynamics: The basics with applications*. McGraw-Hill, 1995.

[47] S. Pirbastami, "CFD SIMULATION OF HEAT ENHANCEMENT IN INTERNALLY HELICAL GROOVED TUBES," Howard R. Hughes College of Engineering, 2011.

[48] G. Chandrasekaran, "3D Printed Heat Exchangers," ARIZONA STATE UNIVERSITY, 2018.

[49] R. Tiruselvam, W. M. Chin, and V. R. Raghavan, "Double tube heat exchanger with novel enhancement: Part II-single phase convective heat transfer," *Heat Mass Transf. und Stoffuebertragung*, vol. 48, no. 8, pp. 1451–1462, 2012.

[50] S. E. Rad, H. Afshin, and B. Farhanieh, "Heat transfer enhancement in shell-and-tube heat exchangers using porous media," *Heat Transf. Eng.*, vol. 36, no. 3, pp. 262–277, 2015.

[51] T. von Karman, "Turbulence," *J. ofthe Aeronaut. Sci.*, vol. 41, p. 1109, 1937.

[52] T. L. B. A. S. L. F. P. I. D. P. Dewitt, *Fundamentals of heat and mass transfer.*, 7th ed. John Wiley & Sons, Inc.

[53] Y. A. Cengel; and A. J. Ghajar, *Heat and Mass Transfer*, Fith. McGraw-Hill Education, 2015.

[54] T. Brahim and A. Jemni, *HEAT EXCHANGERS: CHARACTERISTICS, TYPES AND EMERGING APPLICATIONS*, no. November. New York: Nova Science Publishers, Inc., 2016.

[55] Z. S. Kareem, M. N. Mohd Jaafar, T. M. Lazim, S. Abdullah, and A. F. Abdulwahid,

"Passive heat transfer enhancement review in corrugation," *Exp. Therm. Fluid Sci.*, vol. 68, pp. 22–38, 2015.

[56] N. Uddin, "Turbulence Modeling of Complex Flows in CFD," no. August, p. 60, 2008.

[57] J. Sodja, "Turbulence models in CFD," *Univ. Ljubljana*, no. March, pp. 1–18, 2007.

[58] "STAR-CCM+® Documentation." SIEMENS, STAR CCM+, p. 11519, 2018.

[59] "3 Criteria for Assessing CFD Convergence > ENGINEERING.com." [Online]. Available: https://www.engineering.com/DesignSoftware/DesignSoftwareArticles/ArticleID/9296/3-Criteria-for-Assessing-CFD-Convergence.aspx. [Accessed: 22-Sep-2020].

[60] E. M. Lazar, "POLYHEDRAL CELLS IN NATURAL STRUCTURES." [Online]. Available: http://u.math.biu.ac.il/~mlazar/polyhedral_cells.html.

[61] I. Shukla, S. S. Tupkari, A. K. Raman, and A. N. Mullick, "Wall Y+ approach for dealing with turbulent flow through a constant area duct," *AIP Conf. Proc.*, vol. 1440, no. June, pp. 144–153, 2012.

[62] G. Liu, C. Yang, J. Zhang, H. Zong, B. Xu, and J. Y. Qian, "Internal flow analysis of a heat transfer enhanced tube with a segmented twisted tape insert," *Energies*, vol. 13, no. 1, 2020.

[63] J. Hærvig, K. Sørensen, and T. J. Condra, "On the fully-developed heat transfer enhancing flow field in sinusoidally, spirally corrugated tubes using computational fluid dynamics," *Int. J. Heat Mass Transf.*, vol. 106, no. November, pp. 1051–1062, 2017.

[64] M. Li, "THE PETROLEUM INSTITUTE HEAT TRANSFER AND PRESSURE DROP CHARACTERISTICS OF A SINGLE ENHANCED," The Potroleum Institute, 2015.

[65] L. Vermooten, "Characterization of a titanium coaxial condenser," North West University, 2020.

[66] Z. Jin, B. Liu, F. Chen, Z. Gao, X. Gao, and J. Qian, "International Journal of Heat and Mass Transfer CFD analysis on flow resistance characteristics of six-start spirally corrugated tube," *Int. J. Heat Mass Transf.*, vol. 103, pp. 1198–1207, 2016.

[67] C. Maradiya, J. Vadher, and R. Agarwal, "The heat transfer enhancement techniques

and their Thermal Performance Factor," *Beni-Suef Univ. J. Basic Appl. Sci.*, vol. 7, no. 1, pp. 1–21, 2018.

[68] T. Lemenand, C. Habchi, D. Della Valle, and H. Peerhossaini, "Vorticity and convective heat transfer downstream of a vortex generator," *Int. J. Therm. Sci.*, vol. 125, no. January 2016, pp. 342–349, 2018.

[69] M. Savli, "Turbulence kinetic energy - TKE," *Turbul. Kinet. Energy*, p. 14, 2012.

[70] E. B. van Wyk, "Thermal conductivity of metal additive manufactured parts," North West University, 2019.

[71] Renishaw, "Ti6Al4V ELI-0406 powder for additive manufacturing," vol. 2001, no. Iso 97. pp. 1–3, 2001.

CHAPTER 7: ANNEXURES

7.1 A: EES Code:

```
{Heat Flux}
q_flux= 10000                                  {W/m2}
m_dot_w =0,09                                  {Mass Flow [kg/s]}

q=q_flux*A_outer                               {Convection energy [W]}
A_outer = pi*D_o*L_inc                         {Surface area}
A_surface = pi*D_i*L_inc
A_cross = pi*(D_i/2)^2                         {Cross sectional area}

T_w_o[0] = 20                                  {Inlet water temp}
P_o[0] = 4000                                  {Inlet water pressure [Pa]}


L= 1                                           {Length of tube [m]}
D_i=0,03                                       {Inner diameter [m]}
D_o = 0,05                                     {Outer diameter [m]}
RR = e/D_i                                     {Relative roughness}
e=4,57*10^(-4)                                 {Surface roughness}

Distance[0] = 0                                {For graphs}
L_inc = L/n                                    {Incremental length}
n = 10

Duplicate i=1;n
{Inlet and outlet conditions}
    T_w_i[i] = T_w_o[i-1]                      {Water temp}
    P_i[i] = P_o[i-1]                          {Water pressure}

    Distance[i] = Distance[i-1]+L_inc

{Water properties}
rho[i]=density(Water;T=(T_w_i[i]+T_w_o[i])/2;P=(P_i[i]+P_o[i])/2)
cp[i]=cp(Water;T=(T_w_i[i]+T_w_o[i])/2;P=(P_i[i]+P_o[i])/2)
mu[i]=viscosity(Water;T=(T_w_i[i]+T_w_o[i])/2;P=(P_i[i]+P_o[i])/2)
Pr[i]=prandtl(Water;T=(T_w_i[i]+T_w_o[i])/2;P=(P_i[i]+P_o[i])/2)
k[i]=conductivity(Water;T=(T_w_i[i]+T_w_o[i])/2;P=(P_i[i]+P_o[i])/2)

{Titanium conductivity}
k_Ti[i]=conductivity(Ti_6Al_4V; T= (T_s_inner[i]+T_s_outer[i])/2)

{Water mass flow}
m_dot_w= rho[i]*v[i]*A_cross

{Reynolds number}
Re[i] = (rho[i]*v[i]*D_i)/mu[i]
h_i[i] =if(Re[i];2300; h_w_lam[i];0;h_w_turb[i])

{Convection coefficient}
h_w_turb[i]= (0,023*Re[i]^0,8*Pr[i]^0,4)*(k[i]/D_i)
h_w_lam[i] = 4,36*(k[i]/D_i)
```

```
 {Energy equations}
q =h_i[i]*A_surface*((T_s_inner[i]-T_w_o[i])-(T_s_inner[i]-T_w_i[i]))/(ln((T_s_inner[i]-
T_w_o[i])/(T_s_inner[i]-T_w_i[i])))
q= m_dot_w*cp[i]*(T_w_o[i]-T_w_i[i])
q = (2*pi*L_inc*k_Ti[i]*(T_s_outer[i]-T_s_inner[i]))/(ln((D_o/2)/(D_i/2)))

{Friction factor}
f[i]=moodychart(Re[i]; RR)
 {Pressure loss}
delta_P[i]=f[i]*(rho[i]*(v[i]^2)*L_inc)/(2*D_i)
 delta_P[i] = P_i[i]-P_o[i]

End
q_tot=q*n
T_w_final = T_w_o[n]
P_w_final = P_o[n]
pressure_drop = P_o[0]-P_o[n]
h_avg = sum(h_i[i];i=1;n)/n
k_avg = sum(k[i];i=1;n)/n
```